

IHDG: AN ITERATIVE HDG FRAMEWORK FOR PARTIAL DIFFERENTIAL EQUATIONS. *

SRIRAMKRISHNAN MURALIKRISHNAN*, MINH-BINH TRAN[†], AND TAN BUI-THANH[‡]

Abstract. We present a scalable iterative solver for high-order hybridized discontinuous Galerkin (HDG) discretizations of linear partial differential equations. It is an interplay between domain decomposition methods and HDG discretizations. In particular, the method is a fixed-point approach that requires only independent element-by-element local solves in each iteration. As such, it is well-suited for current and future computing systems with massive concurrencies. We rigorously show the convergence of the proposed method for transport equation, linearized shallow water equation and convection-diffusion equation. For transport equation, the method is convergent regardless of mesh size h and solution order p , and furthermore the convergence rate is independent of the solution order. For linearized shallow water and convection-diffusion equations we show that the convergence is conditional on both h and p . Extensive 2D and 3D numerical results for steady and time-dependent problems are presented to verify the theoretical findings.

Key words. Iterative solvers; Schwarz methods; Hybridized Discontinuous Galerkin methods; Transport equation; shallow water equation; convection-diffusion equation; convergence

AMS subject classifications. 65N30, 65N55, 65N22, 65N12, 65F10

1. Introduction. The discontinuous Galerkin (DG) method was originally developed by Reed and Hill [39] for the neutron transport equation, first analyzed in [25, 28], and then has been extended to other problems governed by partial differential equations (PDEs) [11]. Roughly speaking, DG combines advantages of classical finite volume and finite element methods. In particular, it has the ability to treat solutions with large gradients including shocks, it provides the flexibility to deal with complex geometries, and it is highly parallelizable due to its compact stencil. However, for steady state problems or time-dependent ones that require implicit time-integrators, DG methods typically have many more (coupled) unknowns compared to the other existing numerical methods, and hence more expensive in general.

In order to mitigate the computational expense associated with DG methods, Cockburn, coauthors, and others have introduced hybridizable (also known as hybridized) discontinuous Galerkin (HDG) methods for various types of PDEs including Poisson-type equation [7, 9, 10, 13, 26, 34], Stokes equation [8, 35], Euler and Navier-Stokes equations, wave equations [12, 21, 29, 33, 36–38], to name a few. The upwind HDG framework proposed in [3–5] provides a unified and a systematic construction of HDG methods for a large class of PDEs. In HDG discretizations, the coupled unknowns are single-valued traces introduced on the mesh skeleton, i.e. the faces, and the resulting matrix is substantially smaller and sparser compared to standard DG approaches. Once they are solved for, the usual DG unknowns can be recovered in an element-by-element fashion, completely independent of each other. Nevertheless, the trace system is still a bottleneck for practically large-scale applications, where

¹Department of Aerospace Engineering and Engineering Mechanics, The University of Texas at Austin, Austin, TX 78712, USA.

²Department of Mathematics, University of Wisconsin, Madison, WI 53706, USA.

³Department of Aerospace Engineering and Engineering Mechanics, and the Institute for Computational Engineering and Sciences, The University of Texas at Austin, Austin, TX 78712, USA.

*This research was partially supported by DOE grants DE-SC0010518 and DE-SC0011118, NSF Grant RNMS (Ki-Net) 1107444, ERC Advanced Grant FP7-246775 NUMERIWAVES and ERC Advanced Grant DYCON : Dynamic Control. We are grateful for the supports.

complex and high-fidelity simulations involving features with a large range of spatial and temporal scales are necessary.

Meanwhile, Schwarz-type domain decomposition methods (DDMs) have been introduced as procedures to parallelize and solve partial differential equations efficiently, in which each iteration involves the solutions of the original equation on smaller subdomains [30–32]. Schwarz waveform relaxation methods and optimized Schwarz methods [2, 15, 16, 22, 23, 41, 42] have attracted substantial attention over the past decades since they can be adapted to the underlying physics, and thus lead to efficient parallel solvers for challenging problems. We view the iHDG method as an extreme DDM approach in which each subdomain is an element. For current DDM methods, decomposing the computational domain into smaller subdomains encounters difficulties when the subdomains have cross-points [18] or irregular shapes [17]; moreover, the geometry of the decomposition also has a profound influence on the method [14]. We design the iHDG method to have a two-tier parallelism to adapt to current and future computing systems: a coarse-grained parallelism on subdomains, and a fine-grained parallelism on elements level within each subdomain. Unlike existing approaches, our method does not rely on any specific partition of the computational domain, and hence is independent of the geometry of the decomposition.

While either HDG community or DDM community can contribute individually towards advancing its own field, the potential for breakthroughs may lie in bringing together the advances from both sides and in exploiting opportunities at their interfaces. In [16], Schwarz methods for the hybridizable interior penalty method have been introduced for elliptic PDEs in the second order form. The methods are proposed for two sub-domains, entirely at an algebraic level. In this paper, we blend the HDG method and optimized Schwarz idea to produce efficient and scalable iterative solvers for HDG discretizations. One of the main features of the proposed approach is that it is provably convergent. From a linear algebra point of view, the method can be understood as a block Gauss-Seidel iterative solver. It can be also viewed as a fixed-point approach that requires only independent element-by-element local solves in each iteration. As such, it is well-suited for current and future computing systems with massive concurrencies. We rigorously show that our proposed methods are convergent using an energy approach. Furthermore the convergence rate is independent of the solution order for hyperbolic PDEs. The theoretical findings will be verified on various 2D and 3D numerical results for steady and time-dependent problems.

The structure of paper is organized as follows. Section 2 introduces the iHDG algorithm for an abstract system of PDEs discretized by the upwind HDG discretization [3]. The convergence of the iHDG algorithm for scalar and system of hyperbolic PDEs is proved in section 3 using an energy approach. In section 4 the convection-diffusion PDE is considered in the first order form and the conditions for the convergence of the iHDG algorithm are stated and proved. Section 5 presents various steady and time dependent examples, in both two and three spatial dimensions, to support the theoretical findings. We finally conclude the paper in section 6 and discuss future research directions.

2. The idea of iHDG. In this section we first briefly review the upwind HDG framework for a general system of linear PDEs, and then present the main idea behind the iHDG approach. To begin, let us consider the following system

$$\sum_{k=1}^d \partial_k \mathbf{F}_k(\mathbf{u}) + \mathbf{C}\mathbf{u} := \sum_{k=1}^d \partial_k (\mathbf{A}_k \mathbf{u}) + \mathbf{C}\mathbf{u} = \mathbf{f}, \quad \text{in } \Omega, \quad (2.1)$$

where d is the spatial dimension (which, for the clarity of the exposition, is assumed to be $d = 3$ whenever a particular value of the dimension is of concern, but the result is also valid for $d = \{1, 2\}$), \mathbf{F}_k the k th component of the flux vector (or tensor) \mathbf{F} , \mathbf{u} the unknown solution with values in \mathbb{R}^m , and \mathbf{f} the forcing term. The matrices \mathbf{A}_k and \mathbf{C} are assumed to be continuous¹ across Ω . Here, ∂_k is understood as the k th partial derivative. We choose to discretize (2.1) using the HDG method. To that end, let us introduce notations and conventions used in the paper.

Let us partition $\Omega \in \mathbb{R}^d$, an open and bounded domain, into N_{el} non-overlapping elements $K_j, j = 1, \dots, N_{\text{el}}$ with Lipschitz boundaries such that $\Omega_h := \cup_{j=1}^{N_{\text{el}}} K_j$ and $\bar{\Omega} = \bar{\Omega}_h$. Here, h is defined as $h := \max_{j \in \{1, \dots, N_{\text{el}}\}} \text{diam}(K_j)$. We denote the skeleton of the mesh by $\mathcal{E}_h := \cup_{j=1}^{N_{\text{el}}} \partial K_j$, the set of all (uniquely defined) faces e . We conventionally identify \mathbf{n}^- as the normal vector on the boundary ∂K of element K (also denoted as K^-) and $\mathbf{n}^+ = -\mathbf{n}^-$ as the normal vector of the boundary of a neighboring element (also denoted as K^+). Furthermore, we use \mathbf{n} to denote either \mathbf{n}^- or \mathbf{n}^+ in an expression that is valid for both cases, and this convention is also used for other quantities (restricted) on a face $e \in \mathcal{E}_h$. For the sake of convenience, we denote by \mathcal{E}_h^∂ the sets of all boundary faces on $\partial\Omega$, by $\mathcal{E}_h^\circ := \mathcal{E}_h \setminus \mathcal{E}_h^\partial$ the set of all interior faces, and $\partial\Omega_h := \{\partial K : K \in \Omega_h\}$.

For simplicity in writing we define $(\cdot, \cdot)_K$ as the L^2 -inner product on a domain $K \in \mathbb{R}^d$ and $\langle \cdot, \cdot \rangle_K$ as the L^2 -inner product on a domain K if $K \in \mathbb{R}^{d-1}$. We shall use $\|\cdot\|_K := \|\cdot\|_{L^2(K)}$ as the induced norm for both cases and the particular value of K in a context will indicate which inner product the norm is coming from. We also denote the ε -weighted norm of a function u as $\|u\|_{\varepsilon, K} := \|\sqrt{\varepsilon}u\|_K$ for any positive ε . We shall use boldface lowercase letters for vector-valued functions and in that case the inner product is defined as $(\mathbf{u}, \mathbf{v})_K := \sum_{i=1}^m (\mathbf{u}_i, \mathbf{v}_i)_K$, and similarly $\langle \mathbf{u}, \mathbf{v} \rangle_K := \sum_{i=1}^m \langle \mathbf{u}_i, \mathbf{v}_i \rangle_K$, where m is the number of components ($\mathbf{u}_i, i = 1, \dots, m$) of \mathbf{u} . Moreover, we define $(\mathbf{u}, \mathbf{v})_\Omega := \sum_{K \in \Omega_h} (\mathbf{u}, \mathbf{v})_K$ and $\langle \mathbf{u}, \mathbf{v} \rangle_{\mathcal{E}_h} := \sum_{e \in \mathcal{E}_h} \langle \mathbf{u}, \mathbf{v} \rangle_e$ whose induced (weighted) norms are clear, and hence their definitions are omitted. We employ boldface uppercase letters, e.g. \mathbf{L} , to denote matrices and tensors. In addition, subscripts are used to denote the components of vectors, matrices, and tensors. We conventionally use \mathbf{u} (\mathbf{v} and $\hat{\mathbf{u}}$) for the numerical solution and \mathbf{u}^e for the exact solution.

We define $\mathcal{P}^p(K)$ as the space of polynomials of degree at most p on a domain K . Next, we introduce two discontinuous piecewise polynomial spaces

$$\begin{aligned} \mathbf{V}_h(\Omega_h) &:= \left\{ \mathbf{v} \in [L^2(\Omega_h)]^m : \mathbf{v}|_K \in [\mathcal{P}^p(K)]^m, \forall K \in \Omega_h \right\}, \\ \mathbf{\Lambda}_h(\mathcal{E}_h) &:= \left\{ \boldsymbol{\lambda} \in [L^2(\mathcal{E}_h)]^m : \boldsymbol{\lambda}|_e \in [\mathcal{P}^p(e)]^m, \forall e \in \mathcal{E}_h \right\}, \end{aligned}$$

and similar spaces for $\mathbf{V}_h(K)$ and $\mathbf{\Lambda}_h(e)$ by replacing Ω_h with K and \mathcal{E}_h with e . For scalar-valued functions, we denote the corresponding spaces as

$$\begin{aligned} V_h(\Omega_h) &:= \{v \in L^2(\Omega_h) : v|_K \in \mathcal{P}^p(K), \forall K \in \Omega_h\}, \\ \Lambda_h(\mathcal{E}_h) &:= \{\lambda \in L^2(\mathcal{E}_h) : \lambda|_e \in \mathcal{P}^p(e), \forall e \in \mathcal{E}_h\}. \end{aligned}$$

Following [3], we introduce an upwind HDG discretization for (2.1) as: for each element K , the DG local unknown \mathbf{u} and the extra “trace” unknown $\hat{\mathbf{u}}$ need to satisfy

¹This assumption is not a limitation but for the simplicity of the exposition.

$$-(\mathbf{F}(\mathbf{u}), \nabla \mathbf{v})_K + \langle \hat{\mathbf{F}}(\mathbf{u}, \hat{\mathbf{u}}) \cdot \mathbf{n}, \mathbf{v} \rangle_{\partial K} = (\mathbf{f}, \mathbf{v})_K, \quad \forall \mathbf{v} \in \mathbf{V}_h(K), \quad (2.2a)$$

$$\langle [\hat{\mathbf{F}}(\mathbf{u}, \hat{\mathbf{u}}) \cdot \mathbf{n}], \boldsymbol{\mu} \rangle_e = \mathbf{0}, \quad \forall e \in \mathcal{E}_h^o, \quad \forall \boldsymbol{\mu} \in \boldsymbol{\Lambda}_h(e), \quad (2.2b)$$

where we have defined the “jump” operator $[[(\cdot)]] := (\cdot)^- + (\cdot)^+$, and the HDG flux is defined by

$$\hat{\mathbf{F}} \cdot \mathbf{n} = \mathbf{F}(\mathbf{u}) \cdot \mathbf{n} + |\mathbf{A}|(\mathbf{u} - \hat{\mathbf{u}}), \quad (2.3)$$

with² $\mathbf{A} := \sum_{k=1}^d \mathbf{A}_k \mathbf{n}_k = \mathbf{R} \mathbf{S} \mathbf{R}^{-1}$, and $|\mathbf{A}| := \mathbf{R} |\mathbf{S}| \mathbf{R}^{-1}$.

The key idea behind the iHDG approach is the following. We first solve the conservation condition (2.2b) for $\hat{\mathbf{u}}$ as

$$\langle |\mathbf{A}| \hat{\mathbf{u}}, \boldsymbol{\mu} \rangle_e = \langle [[|\mathbf{A}|(\mathbf{u})]] + [\mathbf{F}(\mathbf{u}) \cdot \mathbf{n}], \boldsymbol{\mu} \rangle_e. \quad (2.4)$$

We then construct an iterative algorithm in which the approximation of the HDG solution at the $(k+1)$ th iteration is governed by the local equation (2.2a) as

$$-(\mathbf{F}(\mathbf{u}^{k+1}), \nabla \mathbf{v})_K + \langle \mathbf{F}(\mathbf{u}^{k+1}) \cdot \mathbf{n} + |\mathbf{A}| \mathbf{u}^{k+1} - |\mathbf{A}| \hat{\mathbf{u}}^k, \mathbf{v} \rangle_{\partial K} = (\mathbf{f}, \mathbf{v})_K, \quad (2.5a)$$

where the trace $\hat{\mathbf{u}}^k$ is computed using information at the k -iteration via (2.4), i.e.,

$$\langle |\mathbf{A}| \hat{\mathbf{u}}^k, \boldsymbol{\mu} \rangle_{\partial K} = \langle [[|\mathbf{A}|(\mathbf{u}^k)]] + [\mathbf{F}(\mathbf{u}^k) \cdot \mathbf{n}], \boldsymbol{\mu} \rangle_{\partial K}. \quad (2.5b)$$

Algorithm 1 summarizes the iHDG approach.

Algorithm 1 The iHDG approach.

Ensure: Given initial guess \mathbf{u}^0 , compute the initial trace $\hat{\mathbf{u}}^0$ using (2.5b).

- 1: **while** not converged **do**
 - 2: Solve the local equation (2.5a) for \mathbf{u}^{k+1} using trace $\hat{\mathbf{u}}^k$
 - 3: Compute $\hat{\mathbf{u}}^{k+1}$ using (2.5b).
 - 4: Check convergence. If yes, **exit**, otherwise **set** $k = k + 1$ and **continue**
 - 5: **end while**
-

The appealing feature of iHDG algorithm 1 is that each iteration requires only independent local solve (2.5a) element-by-element, completely independent of each other. The method exploits the structure of HDG in which each local solve is well-defined as long as the trace $\hat{\mathbf{u}}^k$ is given. Furthermore, the global solve via the conservation condition (2.2b) is not needed. Instead, we compute the trace $\hat{\mathbf{u}}^k$ face-by-face (on the mesh skeleton) in parallel, completely independent of each other. The iHDG approach is therefore well-suited for parallel computing systems. It can be viewed as a fixed-point iterative solver by alternating the computation of the local solver (2.2a) and conservation condition (2.2b). It can be also understood as a block Gauss-Seidel approach. However, unlike matrix-based iterative schemes [20, 40], the proposed iHDG method arises from the structure of HDG methods. For that reason, we term it as iterative HDG discretization (iHDG). Unlike the original HDG discretization, it promotes fine-grained parallelism in the conservation constraints. What remains is to show that iHDG converges as the iteration k increases, and this is the focus of Sections 3–4.

²We assume that \mathbf{A} admits an eigen-decomposition, and this is valid for a large class of PDEs of Friedrichs’ type, for example.

3. iHDG methods for hyperbolic PDEs. In this section, we present iHDG methods for scalar and system of hyperbolic PDEs. For the clarity of the exposition, we consider the transport equation and a linearized shallow water system, and extension of the proposed approach to other hyperbolic PDEs is straightforward. To begin, let us consider the transport equation

$$\boldsymbol{\beta} \cdot \nabla u^e = f \quad \text{in } \Omega, \quad (3.1a)$$

$$u^e = g \quad \text{on } \partial\Omega^-, \quad (3.1b)$$

where $\partial\Omega^-$ is the inflow part of the boundary $\partial\Omega$. An upwind HDG discretization [3] for (3.1) consists of the following local equation for each element K

$$-(u, \nabla \cdot (\boldsymbol{\beta} v))_K + \langle \boldsymbol{\beta} \cdot \mathbf{n} u + |\boldsymbol{\beta} \cdot \mathbf{n}| (u - \hat{u}), v \rangle_{\partial K} = (f, v)_K, \quad \forall v \in V_h(K), \quad (3.2)$$

and conservation conditions on all edges e in the mesh skeleton \mathcal{E}_h :

$$\langle [\boldsymbol{\beta} \cdot \mathbf{n} u + |\boldsymbol{\beta} \cdot \mathbf{n}| (u - \hat{u})], \mu \rangle_e = 0, \quad \forall \mu \in \Lambda_h(e). \quad (3.3)$$

Applying the iHDG algorithm 1 to the upwind HDG method (3.2)–(3.3) we obtain the approximate solution u^{k+1} at the $(k+1)$ th iteration restricted on each element K via the following independent local solve: $\forall v \in V_h(K)$,

$$-(u^{k+1}, \nabla \cdot (\boldsymbol{\beta} v))_K + \langle \boldsymbol{\beta} \cdot \mathbf{n} u^{k+1} + |\boldsymbol{\beta} \cdot \mathbf{n}| (u^{k+1} - \hat{u}^k), v \rangle_{\partial K} = (f, v)_K, \quad (3.4)$$

where the trace \hat{u}^k is computed using information from the previous iteration as

$$\hat{u}^k := \{ \{ u^k \operatorname{sgn}(\boldsymbol{\beta} \cdot \mathbf{n}) \} \} + \{ \{ u^k \} \}. \quad (3.5)$$

Next we study the convergence of the iHDG method (3.4)–(3.5). Since (3.1) is linear, it is sufficient to show that iHDG converges for the homogeneous equation with zero forcing f and zero boundary condition g . Let us define ∂K^{out} as the outflow part of ∂K , i.e. $\boldsymbol{\beta} \cdot \mathbf{n} \geq 0$ on ∂K^{out} , and ∂K^{in} as the inflow part of ∂K , i.e. $\boldsymbol{\beta} \cdot \mathbf{n} < 0$ on ∂K^{in} .

THEOREM 3.1. *Assume $-\nabla \cdot \boldsymbol{\beta} \geq \alpha > 0$, i.e. (3.1) is well-posed. The above iHDG iterations for homogeneous transport equation (3.1) converge exponentially with respect to the number of iterations k . In particular, there exist $J \leq N_{el}$ such that*

$$\sum_{K \in \Omega_h} \|u^k\|_{-\frac{\nabla \cdot \boldsymbol{\beta}}{2}, K}^2 + \|u^k\|_{|\boldsymbol{\beta} \cdot \mathbf{n}|, \partial K^{\text{out}}}^2 \leq \frac{c(k)}{2^k} \|u^0\|_{|\boldsymbol{\beta} \cdot \mathbf{n}|, \mathcal{E}_h}^2, \quad (3.6)$$

where $c(k)$ is a polynomial in k of order at most J and is independent of h and p .

Proof. Taking $v = u^{k+1}$ in (3.4) and applying homogeneous forcing condition yield

$$-(u^{k+1}, \nabla \cdot (\boldsymbol{\beta} u^{k+1}))_K + \langle \boldsymbol{\beta} \cdot \mathbf{n} u^{k+1} + |\boldsymbol{\beta} \cdot \mathbf{n}| (u^{k+1} - \hat{u}^k), u^{k+1} \rangle_{\partial K} = 0. \quad (3.7)$$

A simple integration by parts shows that

$$(u^{k+1}, \nabla \cdot (\boldsymbol{\beta} u^{k+1}))_K = \left(u^{k+1}, \frac{\nabla \cdot \boldsymbol{\beta}}{2} u^{k+1} \right)_K + \frac{1}{2} \langle \boldsymbol{\beta} \cdot \mathbf{n} u^{k+1}, u^{k+1} \rangle_{\partial K}. \quad (3.8)$$

Therefore, we can rewrite (3.7) as

$$\|u^{k+1}\|_{-\frac{\nabla \cdot \boldsymbol{\beta}}{2}, K}^2 + \left\langle \left(|\boldsymbol{\beta} \cdot \mathbf{n}| + \frac{1}{2} \boldsymbol{\beta} \cdot \mathbf{n} \right) u^{k+1}, u^{k+1} \right\rangle_{\partial K} = \langle |\boldsymbol{\beta} \cdot \mathbf{n}| \hat{u}^k, u^{k+1} \rangle_{\partial K}. \quad (3.9)$$

On the other hand, (3.5) is equivalent to

$$\hat{u}^k = \begin{cases} u^k & \text{on } \partial K^{\text{out}} \\ u_{\text{ext}}^k & \text{on } \partial K^{\text{in}} \end{cases}, \quad (3.10)$$

where u_{ext}^k is either the physical boundary condition or the solution of the neighbor element that shares the same inflow boundary ∂K^{in} .

Rewriting (3.9) in terms of ∂K^{in} and ∂K^{out} , we obtain

$$\begin{aligned} & \|u^{k+1}\|_{-\frac{\nabla \cdot \beta}{2}, K}^2 + \left\langle \frac{3}{2} |\beta \cdot \mathbf{n}| u^{k+1}, u^{k+1} \right\rangle_{\partial K^{\text{out}}} + \left\langle \frac{1}{2} |\beta \cdot \mathbf{n}| u^{k+1}, u^{k+1} \right\rangle_{\partial K^{\text{in}}} \\ &= \langle |\beta \cdot \mathbf{n}| u^k, u^{k+1} \rangle_{\partial K^{\text{out}}} + \langle |\beta \cdot \mathbf{n}| u_{\text{ext}}^k, u^{k+1} \rangle_{\partial K^{\text{in}}}. \end{aligned}$$

By Cauchy-Schwarz inequality we have

$$\begin{aligned} & \|u^{k+1}\|_{-\frac{\nabla \cdot \beta}{2}, K}^2 + \left\langle \frac{3}{2} |\beta \cdot \mathbf{n}| u^{k+1}, u^{k+1} \right\rangle_{\partial K^{\text{out}}} + \left\langle \frac{1}{2} |\beta \cdot \mathbf{n}| u^{k+1}, u^{k+1} \right\rangle_{\partial K^{\text{in}}} \\ & \leq \frac{1}{2} \langle |\beta \cdot \mathbf{n}| u^k, u^k \rangle_{\partial K^{\text{out}}} + \frac{1}{2} \langle |\beta \cdot \mathbf{n}| u^{k+1}, u^{k+1} \rangle_{\partial K^{\text{out}}} \\ & \quad + \frac{1}{2} \langle |\beta \cdot \mathbf{n}| u_{\text{ext}}^k, u_{\text{ext}}^k \rangle_{\partial K^{\text{in}}} + \frac{1}{2} \langle |\beta \cdot \mathbf{n}| u^{k+1}, u^{k+1} \rangle_{\partial K^{\text{in}}}, \end{aligned}$$

which implies

$$\|u^{k+1}\|_{-\frac{\nabla \cdot \beta}{2}, K}^2 + \|u^{k+1}\|_{|\beta \cdot \mathbf{n}|, \partial K^{\text{out}}}^2 \leq \frac{1}{2} \left\{ \|u^k\|_{|\beta \cdot \mathbf{n}|, \partial K^{\text{out}}}^2 + \|u_{\text{ext}}^k\|_{|\beta \cdot \mathbf{n}|, \partial K^{\text{in}}}^2 \right\}. \quad (3.11)$$

Consider the set \mathcal{K}^1 of all elements K such that ∂K^{in} is a subset of the physical inflow boundary $\partial \Omega^{\text{in}}$ on which we have $u_{\text{ext}}^k = 0$ for all $k \in \mathbb{N}$. We obtain from (3.11) that

$$\|u^{k+1}\|_{-\frac{\nabla \cdot \beta}{2}, K}^2 + \|u^{k+1}\|_{|\beta \cdot \mathbf{n}|, \partial K^{\text{out}}}^2 \leq \frac{1}{2} \|u^k\|_{|\beta \cdot \mathbf{n}|, \partial K^{\text{out}}}^2, \quad (3.12)$$

which implies

$$\|u^{k+1}\|_{|\beta \cdot \mathbf{n}|, \partial K^{\text{out}}}^2 \leq \frac{1}{2} \|u^k\|_{|\beta \cdot \mathbf{n}|, \partial K^{\text{out}}}^2 \leq \dots \leq \frac{1}{2^{k+1}} \|u^0\|_{|\beta \cdot \mathbf{n}|, \partial K^{\text{out}}}^2. \quad (3.13)$$

From (3.12) and (3.13) we also have

$$\|u^{k+1}\|_{-\frac{\nabla \cdot \beta}{2}, K}^2 \leq \frac{1}{2^{k+1}} \|u^0\|_{|\beta \cdot \mathbf{n}|, \partial K^{\text{out}}}^2. \quad (3.14)$$

Next, let us define $\Omega_h^1 := \Omega_h$ and

$$\Omega_h^2 := \Omega_h^1 \setminus \mathcal{K}^1.$$

Consider the set \mathcal{K}^2 of all K in Ω_h^2 such that ∂K^{in} is either (possibly partially) a subset of the physical inflow boundary $\partial \Omega^{\text{in}}$ or (possibly partially) a subset of the outflow boundary of elements in \mathcal{K}^1 . This implies, on $\partial K^{\text{in}} \in \mathcal{K}^2$, u_{ext}^k either is zero for all $k \in \mathbb{N} \setminus \{1\}$ or satisfies the bound

$$\|u_{\text{ext}}^k\|_{|\beta \cdot \mathbf{n}|, \partial K^{\text{in}}}^2 \leq \frac{1}{2^k} \|u_{\text{ext}}^0\|_{|\beta \cdot \mathbf{n}|, \partial K^{\text{in}}}^2. \quad (3.15)$$

Combining (3.11) and (3.15), we obtain

$$\|u^{k+1}\|_{|\beta \cdot \mathbf{n}|, \partial K^{\text{out}}}^2 \leq \frac{1}{2^{k+1}} \left\{ \|u^0\|_{|\beta \cdot \mathbf{n}|, \partial K^{\text{out}}}^2 + (k+1) \|u_{\text{ext}}^0\|_{|\beta \cdot \mathbf{n}|, \partial K^{\text{in}}}^2 \right\}, \quad (3.16)$$

which, together with (3.11), leads to

$$\|u^{k+1}\|_{-\frac{\nabla \cdot \beta}{2}, K}^2 \leq \frac{1}{2^{k+1}} \left\{ \|u^0\|_{|\beta \cdot \mathbf{n}|, \partial K^{\text{out}}}^2 + (k+1) \|u_{\text{ext}}^0\|_{|\beta \cdot \mathbf{n}|, \partial K^{\text{in}}}^2 \right\}. \quad (3.17)$$

Note that in order to control the trace of u^{k+1} on the inflow boundary ∂K^{in} we can apply an inverse trace inequality [43] on (3.17) to obtain

$$\frac{2h}{d(p+1)(p+2)} \|u^{k+1}\|_{|\beta \cdot \mathbf{n}|, \partial K^{\text{in}}}^2 \leq \frac{1}{2^{k+1}} \left\{ \|u^0\|_{|\beta \cdot \mathbf{n}|, \partial K^{\text{out}}}^2 + (k+1) \|u_{\text{ext}}^0\|_{|\beta \cdot \mathbf{n}|, \partial K^{\text{in}}}^2 \right\}.$$

where d is, again, the spatial dimension of the problem. Now defining Ω_h^i and \mathcal{K}^i recursively, and repeating the above arguments conclude the proof. \square

We are in the position to discuss the convergence of the k th iterative solution to the exact solution u^e . For sufficiently smooth exact solution, e.g. $u^e|_K \in H^s(K)$, $s > 3/2$, we assume the following standard convergence result of DG (HDG) methods for transport equation: let $\sigma = \min\{p+1, s\}$, we have

$$\|u - u^e\|_{\Omega_h}^2 \leq C \frac{h^{2\sigma-1}}{p^{2s-1}} \|u^e\|_{H^s(\Omega_h)}^2, \quad (3.18)$$

and we refer the readers to, for example, [3, 25] for a proof.

COROLLARY 3.2. *Suppose the exact solution u^e is sufficiently smooth, i.e. $u^e|_K \in H^s(K)$, $s > 3/2$, then there exists a constant C independent of k, h and p such that*

$$\|u^k - u^e\|_{\Omega_h}^2 \leq C \left(\frac{c(k)}{2^k} \|u^0\|_{|\beta \cdot \mathbf{n}|, \mathcal{E}_h}^2 + \frac{h^{2\sigma-1}}{p^{2s-1}} \|u^e\|_{H^s(\Omega_h)}^2 \right),$$

where $c(k)$ is a polynomial in k of order at most N_{el} and is independent of h and p .

Proof. The result is a direct consequence of the result from Theorem 3.1, the HDG (DG) convergence result (3.18), and the triangle inequality. \square

REMARK 3.3. *For time-dependent transport equation, we discretize the spatial operator using HDG and time using backward Euler method (or Crank-Nicholson method). The iHDG approach in this case is almost identical to the one for steady state equation except that we now have an additional L^2 -term $(u^{k+1}, v)_K / \Delta t$ in the local equation (3.4). This improves the convergence of iHDG. Indeed, the convergence analysis is almost identical except we now have $\|u^{k+1}\|_{-\nabla \cdot \beta / 2 + 1 / \Delta t, K}^2$ instead of $\|u^{k+1}\|_{-\nabla \cdot \beta / 2, K}^2$ in (3.11).*

We next consider the following system of linear hyperbolic PDEs arisen from the oceanic linearized shallow water system [19]:

$$\frac{\partial}{\partial t} \begin{pmatrix} \phi \\ \Phi u \\ \Phi v \end{pmatrix} + \frac{\partial}{\partial x} \begin{pmatrix} \Phi u \\ \Phi \phi \\ 0 \end{pmatrix} + \frac{\partial}{\partial y} \begin{pmatrix} \Phi v \\ 0 \\ \Phi \phi \end{pmatrix} = \begin{pmatrix} 0 \\ f\Phi v - \gamma\Phi u + \frac{\tau_x}{\rho} \\ -f\Phi u - \gamma\Phi v + \frac{\tau_y}{\rho} \end{pmatrix} \quad (3.19)$$

where $\phi = gH$ is the geopotential height with g and H being the gravitational constant and the perturbation of the free surface height, $\Phi > 0$ is a constant mean

flow geopotential height, $\boldsymbol{\vartheta} := (u, v)$ is the perturbed velocity, $\gamma \geq 0$ is the bottom friction, $\boldsymbol{\tau} := (\tau_x, \tau_y)$ is the wind stress, and ρ is the density of the water. Here, $f = f_0 + \beta(y - y_m)$ is the Coriolis parameter, where f_0 , β , and y_m are given constants.

Again, for simplicity of the exposition and analysis, let us employ the backward Euler discretization for temporal derivatives and HDG for spatial ones. Since the unknowns of interest are those at the $(m+1)$ th time step, we can suppress the time index for the clarity of the exposition. Furthermore, since the system (3.19) is linear, a similar argument as above shows that it is sufficient to consider homogeneous system with zero initial condition, boundary condition, and forcing. Also here we consider the case of $\boldsymbol{\tau} = 0$. Applying the iHDG algorithm 1 to the homogeneous system gives

$$\left(\frac{\phi^{k+1}}{\Delta t}, \varphi_1\right)_K - \left(\Phi \boldsymbol{\vartheta}^{k+1}, \nabla \varphi_1\right)_K + \left\langle \Phi \boldsymbol{\vartheta}^{k+1} \cdot \mathbf{n} + \sqrt{\Phi} (\phi^{k+1} - \hat{\phi}^k), \varphi_1 \right\rangle_{\partial K} = 0, \quad (3.20a)$$

$$\left(\frac{\Phi u^{k+1}}{\Delta t}, \varphi_2\right)_K - \left(\Phi \phi^{k+1}, \frac{\partial \varphi_2}{\partial x}\right)_K + \left\langle \Phi \hat{\phi}^k \mathbf{n}_1, \varphi_2 \right\rangle_{\partial K} = (f \Phi v^{k+1} - \gamma \Phi u^{k+1}, \varphi_2)_K, \quad (3.20b)$$

$$\left(\frac{\Phi v^{k+1}}{\Delta t}, \varphi_3\right)_K - \left(\Phi \phi^{k+1}, \frac{\partial \varphi_3}{\partial y}\right)_K + \left\langle \Phi \hat{\phi}^k \mathbf{n}_2, \varphi_3 \right\rangle_{\partial K} = (-f \Phi u^{k+1} - \gamma \Phi v^{k+1}, \varphi_3)_K, \quad (3.20c)$$

where φ_1, φ_2 and φ_3 are the test functions, and

$$\hat{\phi}^k = \{\{\phi^k\}\} + \sqrt{\Phi} \{\{\boldsymbol{\vartheta}^k \cdot \mathbf{n}\}\}.$$

Our goal is to show that $(\phi^{k+1}, \Phi \boldsymbol{\vartheta}^{k+1})$ converges to zero. To that end, let us define

$$\mathcal{C} := \frac{\mathcal{A}}{\mathcal{B}}, \quad \mathcal{A} := \max \left\{ \frac{\Phi + \sqrt{\Phi}}{2}, \frac{(1 + \sqrt{\Phi})}{2} \right\}, \quad (3.21)$$

and

$$\mathcal{B} := \min \left\{ \left(\frac{h}{\Delta t(p+1)(p+2)} + \frac{\sqrt{\Phi} - \Phi}{2} \right), \left(\frac{h}{\Delta t(p+1)(p+2)} + \frac{(2\gamma - 1 - \sqrt{\Phi})}{2} \right) \right\}.$$

We also need the following norms:

$$\left\| (\phi^k, \boldsymbol{\vartheta}^k) \right\|_{\Omega_h}^2 := \left\| \phi^k \right\|_{\Omega_h}^2 + \left\| \boldsymbol{\vartheta}^k \right\|_{\Phi, \Omega_h}^2, \quad \left\| (\phi^k, \boldsymbol{\vartheta}^k) \right\|_{\mathcal{E}_h}^2 := \left\| \phi^k \right\|_{\mathcal{E}_h}^2 + \left\| \boldsymbol{\vartheta}^k \right\|_{\Phi, \mathcal{E}_h}^2.$$

THEOREM 3.4. *Assume that the mesh size h , the time step Δt and the solution order p are chosen such that $\mathcal{B} > 0$ and $\mathcal{C} < 1$, then the approximate solution at the k th iteration $(\phi^k, \boldsymbol{\vartheta}^k)$ converges to zero, i.e.,*

$$\left\| (\phi^k, \boldsymbol{\vartheta}^k) \right\|_{\mathcal{E}_h}^2 \leq \mathcal{C}^k \left\| (\phi^0, \boldsymbol{\vartheta}^0) \right\|_{\mathcal{E}_h}^2, \quad \left\| (\phi^k, \boldsymbol{\vartheta}^k) \right\|_{\Omega_h}^2 \leq \Delta t \mathcal{A} (\mathcal{C} + 1) \mathcal{C}^{k-1} \left\| (\phi^0, \boldsymbol{\vartheta}^0) \right\|_{\mathcal{E}_h}^2,$$

where \mathcal{C} is defined in (3.21).

Proof. Choosing the test functions $\varphi_1 = \phi^{k+1}$, $\varphi_2 = u^{k+1}$ and $\varphi_3 = v^{k+1}$ in (3.20), integrating the second term in (3.20a) by parts, and then summing equations in (3.20) altogether, we obtain

$$\begin{aligned} \frac{1}{\Delta t} (\phi^{k+1}, \phi^{k+1})_K + \frac{\Phi}{\Delta t} (\boldsymbol{\vartheta}^{k+1}, \boldsymbol{\vartheta}^{k+1})_K + \sqrt{\Phi} \langle \phi^{k+1}, \phi^{k+1} \rangle_{\partial K} + \gamma \Phi \langle \boldsymbol{\vartheta}^{k+1}, \boldsymbol{\vartheta}^{k+1} \rangle_{\partial K} \\ = \sqrt{\Phi} \langle \hat{\phi}^k, \phi^{k+1} \rangle_{\partial K} - \Phi \langle \hat{\phi}^k, \mathbf{n} \cdot \boldsymbol{\vartheta}^{k+1} \rangle_{\partial K}. \end{aligned} \quad (3.22)$$

Summing (3.22) over all elements yields

$$\begin{aligned} \sum_K \frac{1}{\Delta t} (\phi^{k+1}, \phi^{k+1})_K + \frac{\Phi}{\Delta t} (\boldsymbol{\vartheta}^{k+1}, \boldsymbol{\vartheta}^{k+1})_K + \sqrt{\Phi} \langle \phi^{k+1}, \phi^{k+1} \rangle_{\partial K} + \gamma \Phi \langle \boldsymbol{\vartheta}^{k+1}, \boldsymbol{\vartheta}^{k+1} \rangle_{\partial K} \\ = \sum_{e \in \mathcal{E}_h} \sqrt{\Phi} \langle \hat{\phi}^k, \phi^{k+1} \rangle_e - \Phi \langle \hat{\phi}^k, \mathbf{n} \cdot \boldsymbol{\vartheta}^{k+1} \rangle_e \\ = \sum_{e \in \mathcal{E}_h} \left\langle 2\sqrt{\Phi} \left(\{\!\!\{ \phi^k \}\!\!\} + \sqrt{\Phi} \{\!\!\{ \boldsymbol{\vartheta}^k \cdot \mathbf{n} \}\!\!\} \right), \{\!\!\{ \phi^{k+1} \}\!\!\} - \sqrt{\Phi} \{\!\!\{ \boldsymbol{\vartheta}^{k+1} \cdot \mathbf{n} \}\!\!\} \right\rangle_e, \end{aligned}$$

by Cauchy-Schwarz inequality

$$\begin{aligned} \leq \sum_{\partial K} \left[\frac{\Phi + \sqrt{\Phi}}{2} \langle \phi^k, \phi^k \rangle_{\partial K} + \frac{\Phi(1 + \sqrt{\Phi})}{2} \langle \boldsymbol{\vartheta}^k, \boldsymbol{\vartheta}^k \rangle_{\partial K} \right] \\ + \sum_{\partial K} \left[\frac{\Phi + \sqrt{\Phi}}{2} \langle \phi^{k+1}, \phi^{k+1} \rangle_{\partial K} + \frac{\Phi(1 + \sqrt{\Phi})}{2} \langle \boldsymbol{\vartheta}^{k+1}, \boldsymbol{\vartheta}^{k+1} \rangle_{\partial K} \right]. \end{aligned} \quad (3.23)$$

An application of inverse trace inequality [43] gives

$$(\phi^{k+1}, \phi^{k+1})_K \geq \frac{h}{(p+1)(p+2)} \langle \phi^{k+1}, \phi^{k+1} \rangle_{\partial K}, \quad (3.24a)$$

$$(\boldsymbol{\vartheta}^{k+1}, \boldsymbol{\vartheta}^{k+1})_K \geq \frac{h}{(p+1)(p+2)} \langle \boldsymbol{\vartheta}^{k+1}, \boldsymbol{\vartheta}^{k+1} \rangle_{\partial K}. \quad (3.24b)$$

Inequality (3.24), together with (3.23), implies

$$\begin{aligned} \sum_{\partial K} \left[\left(\frac{h}{\Delta t(p+1)(p+2)} + \frac{\sqrt{\Phi} - \Phi}{2} \right) \langle \phi^{k+1}, \phi^{k+1} \rangle_{\partial K} \right. \\ \left. + \left(\frac{h}{\Delta t(p+1)(p+2)} + \frac{(2\gamma - 1 - \sqrt{\Phi})}{2} \right) \langle \Phi \boldsymbol{\vartheta}^{k+1}, \boldsymbol{\vartheta}^{k+1} \rangle_{\partial K} \right] \\ \leq \sum_{\partial K} \left[\frac{\Phi + \sqrt{\Phi}}{2} \langle \phi^k, \phi^k \rangle_{\partial K} + \frac{(1 + \sqrt{\Phi})}{2} \langle \Phi \boldsymbol{\vartheta}^k, \boldsymbol{\vartheta}^k \rangle_{\partial K} \right], \end{aligned} \quad (3.25)$$

which implies

$$\left\| (\phi^{k+1}, \boldsymbol{\vartheta}^{k+1}) \right\|_{\mathcal{E}_h}^2 \leq \mathcal{C} \left\| (\phi^k, \boldsymbol{\vartheta}^k) \right\|_{\mathcal{E}_h}^2,$$

where the constant \mathcal{C} is computed as in (3.21). Therefore

$$\left\| (\phi^{k+1}, \boldsymbol{\vartheta}^{k+1}) \right\|_{\mathcal{E}_h}^2 \leq \mathcal{C}^{k+1} \left\| (\phi^0, \boldsymbol{\vartheta}^0) \right\|_{\mathcal{E}_h}^2. \quad (3.26)$$

On the other hand, inequalities (3.23) and (3.26) imply

$$\left\| \left(\phi^{k+1}, \boldsymbol{\vartheta}^{k+1} \right) \right\|_{\Omega_h}^2 \leq \Delta t \mathcal{A} (C+1) \mathcal{C}^k \left\| \left(\phi^0, \boldsymbol{\vartheta}^0 \right) \right\|_{\mathcal{E}_h}^2$$

and this ends the proof. \square

REMARK 3.5. *The above theorem implies that, in order to have a converged algorithm, we need to have the following relation between Δt , p , and h*

$$\Delta t = \mathcal{O} \left(\frac{h}{(p+1)(p+2)} \right).$$

Unlike the convergent result in Theorem 3.1 for scalar hyperbolic equation, the finding in Theorem 3.4 shows that iHDG is conditionally convergent for system of hyperbolic equations. More specifically, the convergence rate depends on the mesh size h , the time step Δt , and the solution order p . This will be confirmed by numerical results in Section 5.

To show the convergence of the k th iterative solution to the exact solution $(\phi^e, \Phi \boldsymbol{\vartheta}^e)$, we assume that the exact solution is smooth, i.e. $(\phi^e, \Phi \boldsymbol{\vartheta}^e)|_K \in [H^s(K)]^3$, $s > 3/2$. If we define

$$\mathcal{E}^e(t) := \sum_K \left\| \phi^e(t) \right\|_{H^s(K)}^2 + \left\| \boldsymbol{\vartheta}^e(t) \right\|_{\Phi, H^s(K)}^2,$$

results from [6] show that, for $\gamma > 0$ and $\sigma = \min\{p+1, s\}$, we have

$$\left\| (\phi - \phi^e, \Phi \boldsymbol{\vartheta} - \Phi \boldsymbol{\vartheta}^e) \right\|_{\Omega_h}^2 \leq C \Delta t \frac{h^{2\sigma-1}}{p^{2s-1}} \mathcal{E}^e(m\Delta t), \quad (3.27)$$

at the m th time step.

COROLLARY 3.6. *Suppose the exact solution satisfies $(\phi^e, \Phi \boldsymbol{\vartheta}^e)|_K \in [H^s(K)]^3$, $s > 3/2$, then there exists a constant C independent of k, h and p such that*

$$\left\| \left(\phi^k - \phi^e, \Phi \boldsymbol{\vartheta}^k - \Phi \boldsymbol{\vartheta}^e \right) \right\|_{\Omega_h}^2 \leq C \Delta t \left(\mathcal{A} (C+1) \mathcal{C}^{k-1} \left\| \left(\phi^0, \boldsymbol{\vartheta}^0 \right) \right\|_{\mathcal{E}_h}^2 + \frac{h^{2\sigma-1}}{p^{2s-1}} \mathcal{E}^e(m\Delta t) \right),$$

with $\sigma = \min\{p+1, s\}$.

4. iHDG methods for convection-diffusion PDEs.

4.1. First order form. In this section we apply the iHDG algorithm 1 to the following prototype convection-diffusion equation in the first order form

$$\kappa^{-1} \boldsymbol{\sigma}^e + \nabla u^e = 0 \quad \text{in } \Omega, \quad (4.1a)$$

$$\nabla \cdot \boldsymbol{\sigma}^e + \boldsymbol{\beta} \cdot \nabla u^e + \nu u^e = f \quad \text{in } \Omega. \quad (4.1b)$$

We suppose that (4.1) is well-posed, i.e.,

$$\nu - \frac{\nabla \cdot \boldsymbol{\beta}}{2} \geq \lambda > 0. \quad (4.2)$$

An upwind HDG numerical flux [3] is given by

$$\hat{\mathbf{F}} \cdot \mathbf{n} = \begin{bmatrix} \hat{u} \mathbf{n}_1 \\ \hat{u} \mathbf{n}_2 \\ \hat{u} \mathbf{n}_3 \\ \boldsymbol{\sigma} \cdot \mathbf{n} + \boldsymbol{\beta} \cdot \mathbf{n} u + \tau (u - \hat{u}) \end{bmatrix}.$$

Strongly enforcing the conservation condition yields

$$\hat{u} = \frac{1}{\tau^+ + \tau^-} (\llbracket \boldsymbol{\sigma} \cdot \mathbf{n} \rrbracket + \llbracket \boldsymbol{\beta} \cdot \mathbf{n} u \rrbracket + \llbracket \tau u \rrbracket),$$

with τ being chosen as

$$\tau^\pm = \frac{\gamma}{2} (\alpha - \boldsymbol{\beta} \cdot \mathbf{n}^\pm). \quad (4.3)$$

Here, γ and α are some parameters which depends on the type of flux chosen. Similar to the previous sections, it is sufficient to consider the homogeneous problem. Applying the iHDG algorithm 1 we have the following iterative scheme

$$\kappa^{-1} (\boldsymbol{\sigma}^{k+1}, \boldsymbol{\tau})_K - (u^{k+1}, \nabla \cdot \boldsymbol{\tau})_K + \langle \hat{u}^k, \boldsymbol{\tau} \cdot \mathbf{n} \rangle_{\partial K} = 0, \quad (4.4a)$$

$$\begin{aligned} & - (\boldsymbol{\sigma}^{k+1}, \nabla v)_K - (u^{k+1}, \nabla \cdot (\boldsymbol{\beta} v) - \nu v)_K + \\ & \langle \boldsymbol{\beta} \cdot \mathbf{n} u^{k+1} + \boldsymbol{\sigma}^{k+1} \cdot \mathbf{n} + \tau(u^{k+1} - \hat{u}^k), v \rangle_{\partial K} = 0, \end{aligned} \quad (4.4b)$$

where

$$\hat{u}^k = \frac{\llbracket \boldsymbol{\sigma}^k \cdot \mathbf{n} \rrbracket + \llbracket \boldsymbol{\beta} \cdot \mathbf{n} u^k \rrbracket + \llbracket \tau u^k \rrbracket}{\gamma \alpha}.$$

For $\varepsilon, \gamma, \alpha, h > 0$ given, define

$$\mathcal{C}_1 := \frac{d(p+1)(p+2)}{2h} \frac{3(\|\boldsymbol{\beta} \cdot \mathbf{n}\|_{L^\infty(\partial K)} + \bar{\tau})(\bar{\tau}\varepsilon + 1)}{\gamma^2 \alpha^2 \varepsilon}, \quad \mathcal{C}_4 := \frac{d(p+1)(p+2)}{2h} \frac{\varepsilon}{2}, \quad (4.5)$$

$$\mathcal{C}_2 := \frac{d(p+1)(p+2)}{2h} \frac{3(\bar{\tau}\varepsilon + 1)}{\gamma^2 \alpha^2 \varepsilon}, \quad \mathcal{C}_3 := \frac{d(p+1)(p+2)}{2h} \frac{\bar{\tau} + \|\boldsymbol{\beta} \cdot \mathbf{n}\|_{L^\infty(\partial K)}}{2}. \quad (4.6)$$

THEOREM 4.1. *Suppose that the mesh size h and the solution order p are chosen such that $\kappa^{-1} > \mathcal{C}_4$, $\lambda - \mathcal{C}_3 > 0$, and*

$$\mathcal{D} := \frac{\max\{\mathcal{C}_1, \mathcal{C}_2\}}{\min\{\kappa^{-1} - \mathcal{C}_4, \lambda - \mathcal{C}_3\}} < 1.$$

The algorithm (4.4a)-(4.4b) converges in the following sense

$$\sum_K \left[\|\boldsymbol{\sigma}^k\|_{L^2(K)}^2 + \|u^k\|_{L^2(K)}^2 \right] \leq \sum_K \mathcal{D}^k \left[\|u^0\|_{L^2(K)}^2 + \|\boldsymbol{\sigma}^0\|_{L^2(K)}^2 \right]. \quad (4.7)$$

Proof. Choosing $\boldsymbol{\sigma}^{k+1}$ and u^{k+1} as test functions in (4.4a)-(4.4b), integrating the second terms in both equations by parts, and then summing up the resulting two equations we get

$$\begin{aligned} & \kappa^{-1} (\boldsymbol{\sigma}^{k+1}, \boldsymbol{\sigma}^{k+1})_K + \left(\frac{-\nabla \cdot \boldsymbol{\beta}}{2} u^{k+1}, u^{k+1} \right)_K + \nu (u^{k+1}, u^{k+1})_K - \frac{1}{2} \langle \boldsymbol{\beta} \cdot \mathbf{n} u^{k+1}, u^{k+1} \rangle_{\partial K} \\ & + \langle \hat{u}^k, \boldsymbol{\sigma}^{k+1} \cdot \mathbf{n} \rangle_{\partial K} + \langle \boldsymbol{\beta} \cdot \mathbf{n} u^{k+1} + \tau(u^{k+1} - \hat{u}^k), u^{k+1} \rangle_{\partial K} = 0. \end{aligned} \quad (4.8)$$

Due to the condition (4.2)

$$\begin{aligned} & \kappa^{-1} (\boldsymbol{\sigma}^{k+1}, \boldsymbol{\sigma}^{k+1})_K + \lambda (u^{k+1}, u^{k+1})_K + \langle \tau u^{k+1}, u^{k+1} \rangle_{\partial K} \\ & \leq \langle \tau \hat{u}^k, u^{k+1} \rangle_{\partial K} - \frac{1}{2} \langle \boldsymbol{\beta} \cdot \mathbf{n} u^{k+1}, u^{k+1} \rangle_{\partial K} - \langle \hat{u}^k, \boldsymbol{\sigma}^{k+1} \cdot \mathbf{n} \rangle_{\partial K}. \end{aligned} \quad (4.9)$$

By Cauchy-Schwarz and Young inequalities and the fact that $|\boldsymbol{\beta} \cdot \mathbf{n}| \leq \|\boldsymbol{\beta} \cdot \mathbf{n}\|_{L^\infty(\partial K)}$ and let $\bar{\tau} = \|\tau\|_{L^\infty(\partial K)}$

$$\begin{aligned} & \kappa^{-1} \|\boldsymbol{\sigma}^{k+1}\|_{L^2(K)}^2 + \lambda \|u^{k+1}\|_{L^2(K)}^2 \\ & \leq \frac{\bar{\tau}\varepsilon + 1}{2\varepsilon} \|\hat{u}^k\|_{L^2(\partial K)}^2 + \frac{\bar{\tau} + \|\boldsymbol{\beta} \cdot \mathbf{n}\|_{L^\infty(\partial K)}}{2} \|u^{k+1}\|_{L^2(\partial K)}^2 + \frac{\varepsilon}{2} \|\boldsymbol{\sigma}^{k+1}\|_{L^2(\partial K)}^2. \end{aligned}$$

Therefore

$$\begin{aligned} & \sum_K \left[\kappa^{-1} \|\boldsymbol{\sigma}^{k+1}\|_{L^2(K)}^2 + \lambda \|u^{k+1}\|_{L^2(K)}^2 \right] \leq \sum_{\partial K} \frac{\bar{\tau}\varepsilon + 1}{2\varepsilon} \|\hat{u}^k\|_{L^2(\partial K)}^2 + \\ & \frac{\bar{\tau} + \|\boldsymbol{\beta} \cdot \mathbf{n}\|_{L^\infty(\partial K)}}{2} \|u^{k+1}\|_{L^2(\partial K)}^2 + \frac{\varepsilon}{2} \|\boldsymbol{\sigma}^{k+1}\|_{L^2(\partial K)}^2. \end{aligned} \quad (4.10)$$

By Cauchy-Schwarz inequality

$$\|\hat{u}^k\|_{L^2(\partial K)}^2 \leq \frac{3\|\boldsymbol{\sigma}^k \cdot \mathbf{n}\|_{L^2(\partial K)}^2 + 3\|\boldsymbol{\beta} \cdot \mathbf{n} u^k\|_{L^2(\partial K)}^2 + 3\|\tau u^k\|_{L^2(\partial K)}^2}{\gamma^2 \alpha^2},$$

which implies

$$\begin{aligned} & \sum_{\partial K} \|\hat{u}^k\|_{L^2(\partial K)}^2 \\ & \leq \sum_{\partial K} \frac{6}{\gamma^2 \alpha^2} \|\boldsymbol{\sigma}^k\|_{L^2(\partial K)}^2 + \frac{6(\|\boldsymbol{\beta} \cdot \mathbf{n}\|_{L^\infty(\partial K)} + \bar{\tau})}{\gamma^2 \alpha^2} \|u^k\|_{L^2(\partial K)}^2. \end{aligned} \quad (4.11)$$

Combining (4.10) and (4.11), we get

$$\begin{aligned} & \sum_K \left[\kappa^{-1} \|\boldsymbol{\sigma}^{k+1}\|_{L^2(K)}^2 + \lambda \|u^{k+1}\|_{L^2(K)}^2 \right] \\ & \leq \sum_{\partial K} \left[\frac{3(\bar{\tau}\varepsilon + 1)}{\gamma^2 \alpha^2 \varepsilon} \|\boldsymbol{\sigma}^k\|_{L^2(\partial K)}^2 + \frac{3(\|\boldsymbol{\beta} \cdot \mathbf{n}\|_{L^\infty(\partial K)} + \bar{\tau})(\bar{\tau}\varepsilon + 1)}{\gamma^2 \alpha^2 \varepsilon} \|u^k\|_{L^2(\partial K)}^2 + \right. \\ & \quad \left. + \frac{\bar{\tau} + \|\boldsymbol{\beta} \cdot \mathbf{n}\|_{L^\infty(\partial K)}}{2} \|u^{k+1}\|_{L^2(\partial K)}^2 + \frac{\varepsilon}{2} \|\boldsymbol{\sigma}^{k+1}\|_{L^2(\partial K)}^2 \right]. \end{aligned} \quad (4.12)$$

By the trace inequality (3.24) we infer from (4.12) that

$$\sum_K \left[(\kappa^{-1} - \mathcal{C}_4) \|\boldsymbol{\sigma}^{k+1}\|_{L^2(K)}^2 + (\lambda - \mathcal{C}_3) \|u^{k+1}\|_{L^2(K)}^2 \right] \leq \sum_K \left[\mathcal{C}_1 \|u^k\|_{L^2(K)}^2 + \mathcal{C}_2 \|\boldsymbol{\sigma}^k\|_{L^2(K)}^2 \right],$$

which implies

$$\sum_K \left[\|\boldsymbol{\sigma}^{k+1}\|_{L^2(K)}^2 + \|u^{k+1}\|_{L^2(K)}^2 \right] \leq \sum_K \frac{\max\{\mathcal{C}_1, \mathcal{C}_2\}}{\min\{\kappa^{-1} - \mathcal{C}_4, \lambda - \mathcal{C}_3\}} \left[\|u^k\|_{L^2(K)}^2 + \|\boldsymbol{\sigma}^k\|_{L^2(K)}^2 \right],$$

and this concludes the proof. \square

REMARK 4.2. For time-dependent convection-diffusion equation, we choose to discretize the spatial differential operators using HDG. For the temporal derivative, we use implicit time stepping methods, again with either backward Euler or Crank-Nicolson method for simplicity. The iHDG approach in this case is almost identical to the one for steady state equation except that we now have an additional L^2 -term $(u^{k+1}, v)_K / \Delta t$ in the local equation (4.4b). This improves the convergence of iHDG. Indeed, the convergence analysis is almost identical except we now have $\lambda + 1/\Delta t$ in place of λ .

4.2. Conditions for convergence. In this section we choose specific forms of fluxes and define parameters Q_1 and Q_2 for each flux based on \mathcal{C}_1 to \mathcal{C}_4 in (4.5) and (4.6). The condition for convergence of iHDG from Theorem 4.1 can then be translated as

$$h > \max \{Q_1, Q_2\}.$$

For upwind flux [3] we have $\gamma = 1$ and $\alpha = \sqrt{|\boldsymbol{\beta} \cdot \mathbf{n}|^2 + 4}$ in (4.3). With the choice of $\varepsilon = \mathcal{O}\left(\frac{1}{\alpha - \|\boldsymbol{\beta} \cdot \mathbf{n}\|}\right)$ in (4.5) and (4.6) we obtain³

$$Q_1 = \mathcal{O}\left(\frac{d(p+1)(p+2)}{\lambda} \left[\frac{9}{8} \left\{ 1 - \frac{\|\boldsymbol{\beta} \cdot \mathbf{n}\|^2}{\alpha^2} \right\} + \left\{ \alpha + \frac{\|\boldsymbol{\beta} \cdot \mathbf{n}\|}{2} \right\} \right] \right),$$

$$Q_2 = \mathcal{O}\left(\frac{d(p+1)(p+2)}{\kappa^{-1}} \left[\frac{9}{8} \left\{ 1 - \frac{\|\boldsymbol{\beta} \cdot \mathbf{n}\|^2}{\alpha^2} \right\} + \left\{ \frac{1}{4(\alpha - \|\boldsymbol{\beta} \cdot \mathbf{n}\|)} \right\} \right] \right).$$

In the diffusion dominated regime, Q_2 determines the convergence, while in the convection dominated regime, Q_1 does. Notice that since Q_1 is not a function of κ , the convergence is independent of κ in the convection dominated regime for the upwind flux. This is confirmed in the numerical section 5.3.

For the flux given in Nguyen et. al. [34] (NPC flux) we have $\gamma = 2$ and $\alpha = (|\boldsymbol{\beta} \cdot \mathbf{n}| + \kappa)^{\frac{1+\text{sgn}(\boldsymbol{\beta} \cdot \mathbf{n})}{2}}$ in (4.3). With $\varepsilon = \mathcal{O}\left(\frac{1}{\alpha - \|\boldsymbol{\beta} \cdot \mathbf{n}\|}\right)$ we obtain

$$Q_1 = \mathcal{O}\left(\frac{d(p+1)(p+2)}{\lambda} \left[\frac{\alpha}{4} + 3 \left\{ 1 - \frac{\|\boldsymbol{\beta} \cdot \mathbf{n}\|}{\alpha} \right\} \right] \right),$$

$$Q_2 = \mathcal{O}\left(\frac{d(p+1)(p+2)}{\kappa^{-1}} \left[3 \left\{ 1 - \frac{\|\boldsymbol{\beta} \cdot \mathbf{n}\|}{\alpha} \right\} + \left\{ \frac{1}{4(\alpha - \|\boldsymbol{\beta} \cdot \mathbf{n}\|)} \right\} \right] \right).$$

For this flux, Q_1 also depends on κ (as $\alpha = \alpha(\kappa, \boldsymbol{\beta})$). Hence with decreasing κ , the convergence is improved as the constant in front of Q_1 decreases. For very small κ , we recover the convergence of the pure hyperbolic case. This is shown in the numerical section 5.3. In the diffusion dominated/elliptic regime both upwind flux and NPC one violate the condition $\kappa^{-1} > \mathcal{C}_4$ in Theorem 4.1 for any mesh and diverge. Hence, we introduce a variant of the upwind flux with $\gamma = \frac{(p+1)(p+2)}{h}$ (based on dimensional analysis and the trace inequality) and α same as in the upwind flux in (4.3). With $\varepsilon = \mathcal{O}\left(\frac{h}{(p+1)(p+2)(\alpha - \|\boldsymbol{\beta} \cdot \mathbf{n}\|)}\right)$, Q_1 and Q_2 in this case are given by

$$Q_1 = \mathcal{O}\left(\frac{(p+1)(p+2)}{2\sqrt{\lambda}} \left(\sqrt{d \{ \alpha - \|\boldsymbol{\beta} \cdot \mathbf{n}\| \}} \right) \right),$$

$$Q_2 = \mathcal{O}\left(\frac{9d(p+1)(p+2)}{4\alpha^2\kappa^{-1}} (\alpha - \|\boldsymbol{\beta} \cdot \mathbf{n}\|)^2 \right).$$

This satisfies the necessary condition $\kappa^{-1} > \mathcal{C}_4$ in Theorem 4.1, independent of h and p . However this is also conditionally convergent in the diffusion dominated regime as given by the condition $h > \max \{Q_1, Q_2\}$.

³In this section $\|\boldsymbol{\beta} \cdot \mathbf{n}\| = \|\boldsymbol{\beta} \cdot \mathbf{n}\|_{L^\infty(\partial K)}$.

5. Numerical results. In this section various numerical results supporting the theoretical results are provided for 2D and 3D transport equations, the linearized shallow water equation, and the convection-diffusion equation in different regimes.

5.1. Steady state transport equation. The goal is to verify Theorem 3.1 for the transport equation (3.1) in 2D and 3D settings for the upwind HDG and the NPC fluxes. To begin, let us recall that the stabilization τ of NPC flux is given by

$$\tau = |\boldsymbol{\beta} \cdot \mathbf{n}| \frac{1 + \text{sgn}(\boldsymbol{\beta} \cdot \mathbf{n})}{2} - \boldsymbol{\beta} \cdot \mathbf{n}, \quad (5.1)$$

and the trace \hat{u}^k at the k th iteration is computed as

$$\hat{u}^k = \frac{\{\{\tau u^k\}\} + \{\{\boldsymbol{\beta} \cdot \mathbf{n} u^k\}\}}{\{\{\tau\}\}}.$$

THEOREM 5.1. *Assume $-\nabla \cdot \boldsymbol{\beta} \geq \alpha > 0$, i.e. (3.1) is well-posed. There exists $J \leq N_{el}$ such that the iHDG algorithm with the NPC flux for the homogeneous transport equation converges in J iterations.*⁴

This theorem shows that for scalar hyperbolic equation (3.1), iHDG with the NPC flux converges in finite number of iterations, which is faster than the upwind HDG flux. The reason is that the NPC flux mimics the matching of wave propagation from the inflow to the outflow. However, designing such a scheme for system of hyperbolic equations, such as the linearized shallow water system, does not seem to be tractable due to the interaction of more than one waves. In this sense the upwind HDG flux is more robust, since it is applicable for other system of hyperbolic PDEs as well.

5.1.1. 2D steady state transport equation with discontinuous solution.

We consider the case similar to the one in ([3], [24]) where $f = 0$ and $\boldsymbol{\beta} = (1 + \sin(\pi y/2), 2)$ in (3.1). The domain is $[0, 2] \times [0, 2]$ and the conditions at the inflow boundary are given by

$$g = \begin{cases} 1 & x = 0, 0 \leq y \leq 2 \\ \sin^6(\pi x) & 0 < x \leq 1, y = 0 \\ 0 & 1 \leq x \leq 2, y = 0 \end{cases}.$$

To terminate the iHDG algorithm, we use the following stopping criteria

$$\|u^k - u^{k-1}\|_{L^2} < 10^{-10}, \quad (5.2)$$

i.e., iHDG stops when there is insignificant change between two successive iterations.

The evolution of the iterative solution for the mesh with 1024 elements and solution order 4 using both upwind and NPC fluxes is shown in figure 5.1. In both cases, we observe that the iterative solution evolves from inflow to outflow as the number of iterations increases. As can be seen, iHDG with NPC flux converges faster (in fact in finite number of iterations) as predicted by Theorem 5.1.

The 4th and 5th columns of Table 5.1 show the number of iterations required to converge for both the fluxes with different meshes and solution orders 3 and 4. We observe that the number of iterations is (almost) independent of solution order⁵ for both the fluxes, which is in agreement with the theoretical results in Theorems 3.1 and 5.1. This is important for high-order methods, i.e., the solution order (and hence accuracy) can be increased while keeping the number of iHDG iterations unchanged.

⁴The proof is similar to the proof of Theorem 3.1, and hence is omitted here.

⁵The results for $p = \{1, 2\}$ are not shown, as the number of iterations is very similar that of the $p = \{3, 4\}$ -cases.

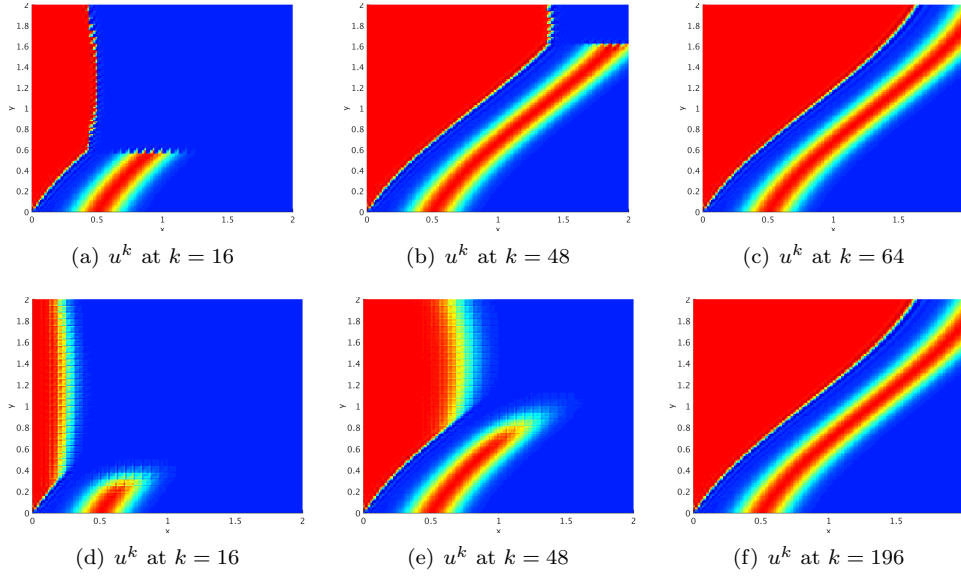


Fig. 5.1: Evolution of the iterative solution for the NPC flux (top row) and the upwind HDG flux (bottom row).

Table 5.1: The number of iterations taken by the iHDG algorithm using NPC and upwind HDG fluxes for transport equation in 2D and 3D settings.

$N_{el}(2D)$	$N_{el}(3D)$	p	2D solution		3D solution	
			Upwind	NPC	Upwind	NPC
16	8	3	65	9	39	7
64	64	3	91	17	49	12
256	512	3	133	33	79	23
1024	4096	3	209	65	136	47
16	8	4	65	9	35	6
64	64	4	87	17	51	12
256	512	4	129	33	83	24
1024	4096	4	196	64	143	48

5.1.2. 3D steady state transport equation with smooth solution. In this example we choose $\beta = (z, x, y)$ in (3.1). Also we take the following exact solution

$$u^e = \frac{1}{\pi} \sin(\pi x) \cos(\pi y) \sin(\pi z).$$

The forcing is selected in such a way that it corresponds to the exact solution. Here the domain is $[0, 1] \times [0, 1] \times [0, 1]$ with faces $x = 0$, $y = 0$ and $z = 0$ as inflow boundaries. A structured hexahedral mesh is used for the simulations. Since we know the exact solution we use the following stopping criteria:

$$||u^k - u_e||_{L^2(\Omega)} - ||u^{k-1} - u_e||_{L^2(\Omega)} < 10^{-10}. \quad (5.3)$$

Figure 5.2 shows the h -convergence of the HDG discretization with the iHDG iterative solver. The convergence is optimal with rate $(p + 1)$ for both fluxes. Figure

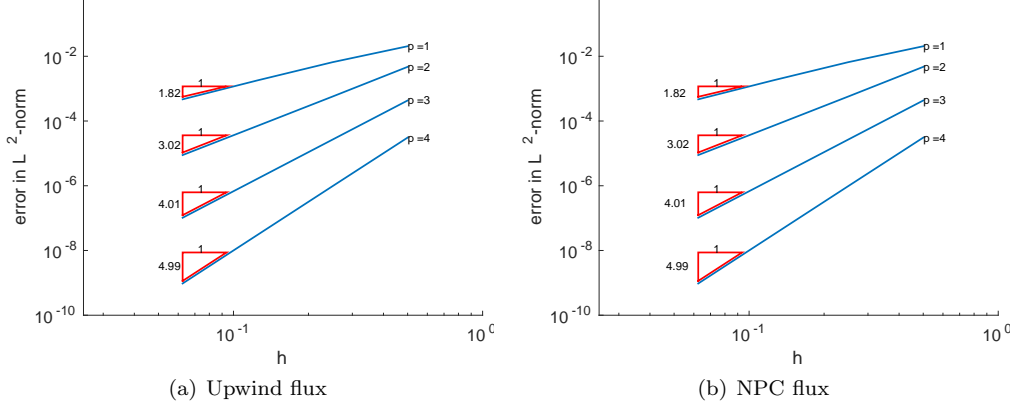


Fig. 5.2: h -convergence of the HDG method using iHDG with upwind and NPC fluxes.

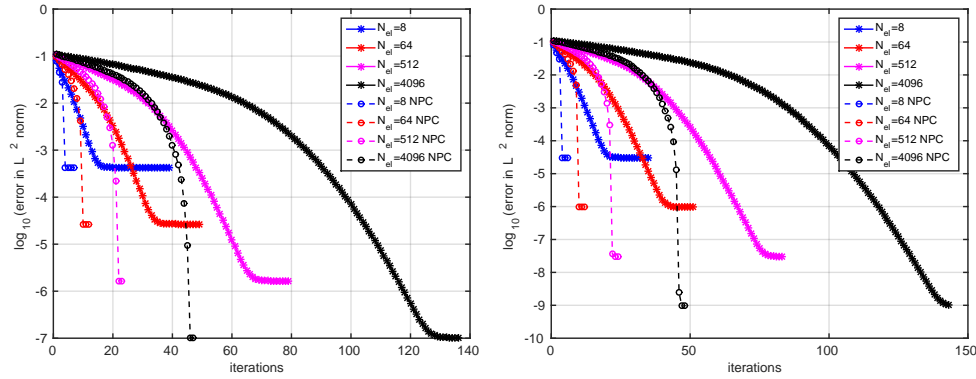


Fig. 5.3: Error history in terms of the number iterations for solution order $p = 3$ (left) and $p = 4$ (right) as the mesh is refined (the number of elements N_{el} increases).

5.3 shows a comparison of the convergence history of the iHDG solver in the log-linear scale. As proved in Theorem 3.1 the iHDG with upwind flux is exponentially convergent with respect to the number of iterations k , while the convergence is attained in finite number of iterations for the NPC flux as predicted in Theorem 5.1. Note that the stagnation region observed near the end of each curve is due to the fact that for a particular mesh size h and solution order p we can achieve only as much accuracy as prescribed by the HDG discretization error and cannot go beyond that. Numerical results for different solution orders⁶ also verify the fact that the convergence of iHDG algorithm is independent of the solution order p . The evolution of the iHDG solution in terms of the number of iterations is shown in Figure 5.4. Again, for scalar transport equation, iHDG automatically matches the solution from the inflow to the outflow. We also record in the 6th and 7th columns of Table 5.1 the number of iterations that the iHDG algorithm took for both the fluxes. As predicted by our theoretical findings, the number of iterations is independent of the solution order.

⁶Here also $p = 1, 2$ results are omitted for brevity.

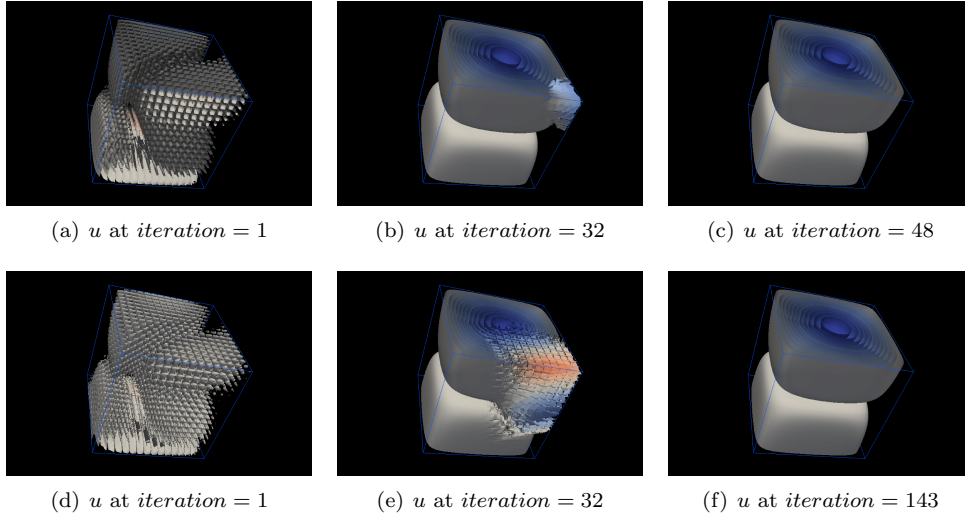


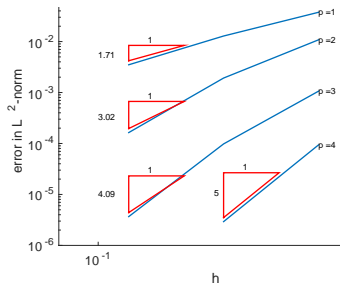
Fig. 5.4: Evolution of the iHDG solution in terms of the number of iterations for the NPC flux (top row) and the upwind HDG flux (bottom row).

5.2. Linearized shallow water equations. In this section we consider equation (3.19) with a linear standing wave, for which, we set $\Phi = 1$, $f = 0$, $\gamma = 0$ (zero bottom friction), $\tau = 0$ (zero wind stress). The domain is $[0, 1] \times [0, 1]$ and wall boundary condition is applied on the domain boundary. The following exact solution [19] is taken

$$\phi = \cos(\pi x) \cos(\pi y) \cos(\sqrt{2}\pi t), \quad (5.4a)$$

$$u = \frac{1}{\sqrt{2}} \sin(\pi x) \cos(\pi y) \sin(\sqrt{2}\pi t), \quad (5.4b)$$

$$v = \frac{1}{\sqrt{2}} \cos(\pi x) \sin(\pi y) \sin(\sqrt{2}\pi t). \quad (5.4c)$$



N_{el}	Solution order			
	1	2	3	4
16	12	13	9	10
64	11	12	7	9
256	9	11	7	8
1024	7	10	7	7

Fig. 5.5: h -convergence of iHDG for 10^5 time steps with $\Delta t = 10^{-6}$ (left) and the number of iHDG iterations per time step with $\Delta t = \frac{h}{(p+1)(p+2)}$ (right) for the linearized shallow water equation.

The iHDG algorithm with upwind HDG flux described in Section 3 along with Crank-Nicolson method for time discretization is employed in this problem. The convergence of the solution is presented in Figure 5.5. Here we have taken $\Delta t = 10^{-6}$ as the stepsize with 10^5 steps. As can be seen, the optimal convergence rate of $(p+1)$

is attained. The number of iterations required per time step in this case is constant and is always equal to 2 for all meshes and solution orders considered. The reason is due to i) a warm-start strategy, that is, the initial guess for each time step is taken as the solution of the previous time step, and ii) small time stepsize.

Following remark 3.5 we choose $\Delta t = \frac{h}{(p+1)(p+2)}$ and report the number of iterations for different meshes and solution orders in Figure 5.5. Clearly, finer mesh and higher solution order require smaller time stepsize, and hence less number of iterations, for the iHDG algorithm to converge.

5.3. Convection-Diffusion Equation. In this section equation (4.1) is considered with the exact solution taken as

$$u^e = \frac{1}{\pi} \sin(\pi x) \cos(\pi y) \sin(\pi z).$$

The forcing is chosen such that it corresponds to the exact solution. The domain is same as the one in section 5.1.2. Dirichlet boundary condition based on the exact solution is applied on the boundary faces and the stopping criteria is same as (5.3).

5.3.1. Convection dominated regime. Let us consider $10^{-3} \leq \kappa \leq 10^{-6}$, $\nu = 1$, and $\beta = (1 + z, 1 + x, 1 + y)$. Since the maximum velocity in this example is $\mathcal{O}(1)$, this represents convection dominated regime. Figure 5.6 shows the optimal h-convergence of the iHDG method with upwind HDG flux⁷ for $\kappa = 10^{-3}$ and $\kappa = 10^{-6}$, respectively. The error history for solution orders $p = \{3, 4\}$ is given in Figure 5.7. As expected, for $\kappa = 10^{-6}$, the iHDG method with either upwind or NPC flux behaves similar to the pure convection case. From table 5.2 the convergence of the upwind iHDG approach remains the same, that is, the number of iterations is insensitive to the diffusion coefficient κ : this is in agreement with the theoretical result in section 4.2. Note that the iHDG approach with NPC flux improves as κ decreases since Q_1 is smaller, and hence leading to faster convergence.

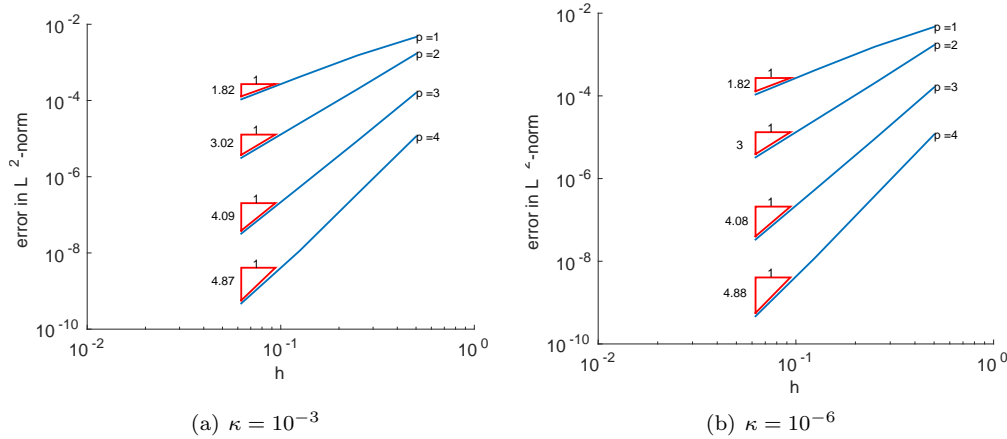


Fig. 5.6: h-convergence of iHDG method with upwind HDG flux for $\kappa = \{10^{-3}, 10^{-6}\}$.

⁷The convergence with NPC flux is similar and hence not shown.

Table 5.2: The number of iHDG iterations for various κ with upwind and NPC fluxes.

h	p	Upwind flux			Nguyen flux		
		$\kappa = 10^{-2}$	$\kappa = 10^{-3}$	$\kappa = 10^{-6}$	$\kappa = 10^{-2}$	$\kappa = 10^{-3}$	$\kappa = 10^{-6}$
0.5	1	24	23	23	10	7	5
0.25	1	30	34	35	21	14	12
0.125	1	50	55	56	94	26	22
0.0625	1	90	94	97	*	52	46
0.5	2	26	24	25	13	8	5
0.25	2	41	42	42	22	15	12
0.125	2	66	67	67	*	26	23
0.0625	2	*	109	110	*	59	46
0.5	3	27	31	31	21	8	5
0.25	3	33	33	38	*	16	12
0.125	3	*	58	60	*	30	24
0.0625	3	*	102	106	*	59	48
0.5	4	26	27	27	73	8	5
0.25	4	50	41	43	*	16	12
0.125	4	*	71	72	*	32	24
0.0625	4	*	123	125	*	71	48

5.3.2. Mixed (hyperbolic-elliptic) regime. In this regime, we take $\kappa = 10^{-2}$, $\nu = 1$, and $\beta = (1+z, 1+x, 1+y)$. Table 5.2 shows that both upwind and NPC fluxes fail to converge for a number of cases (“*” indicates divergence) though the upwind iHDG is more robust. This is due to the violation of the necessary condition $\kappa^{-1} > \mathcal{C}_4$ in Theorem 4.1 for finer meshes. From section 4.2, by choosing $\varepsilon = \mathcal{O}\left(\frac{1}{\alpha - \|\beta \cdot \mathbf{n}\|}\right)$ for the upwind flux (which for this example is $\mathcal{O}(1)$) and $\varepsilon = \mathcal{O}\left(\frac{1}{\alpha}\right)$ for the NPC flux we can estimate the minimum mesh sizes and they are shown in table 5.3. Comparing the second and the third rows of table 5.3 with the first, the third and the sixth columns of table 5.2 we see that the numerical results agree with the theoretical estimates.

Table 5.3: Theoretical estimates on the minimum mesh size for convergence of upwind and NPC fluxes for $\kappa = 0.01$ from section 4.2.

Flux	$p = 1$	$p = 2$	$p = 3$	$p = 4$
Upwind	$h > 0.045$	$h > 0.09$	$h > 0.15$	$h > 0.225$
NPC	$h > 0.09$	$h > 0.18$	$h > 0.3$	$h > 0.45$

5.3.3. Diffusion regime (elliptic equation). As an example for the diffusion limit, we take $\beta = 0$ and $\kappa = 1$. In order to verify the conditional convergence in section 4.2, we choose three different values of ν in the set $\{1, 10, 100\}$. Recall in section 4.2 that neither the upwind flux nor the NPC flux converges for $\kappa = 1$ and $\beta = 0$ (pure diffusion regime). Thus, we consider only the HDG flux with $\tau = \frac{(p+1)(p+2)}{2h}(\alpha - \beta \cdot \mathbf{n})$, which in this case reduces to $\tau = \frac{(p+1)(p+2)}{h}$. The stopping criteria is taken as in (5.3).

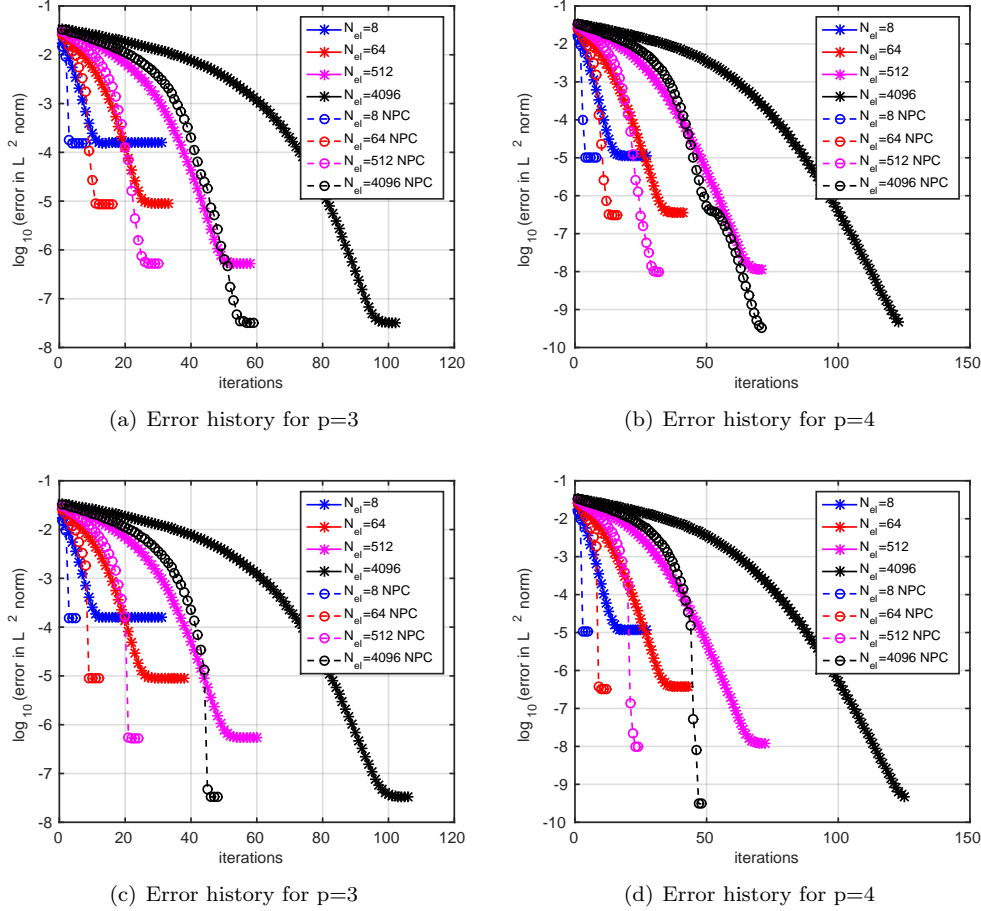


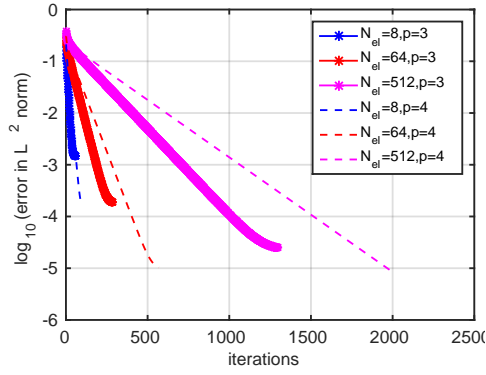
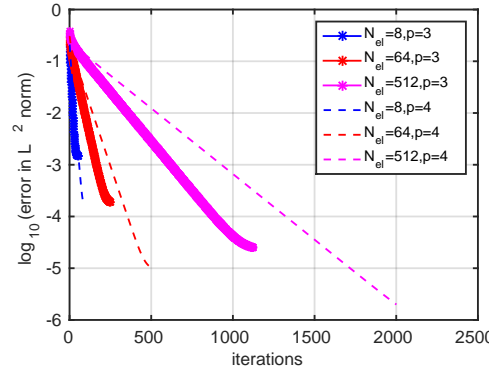
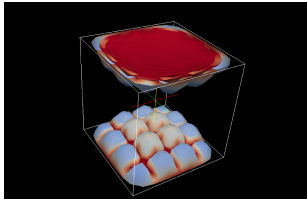
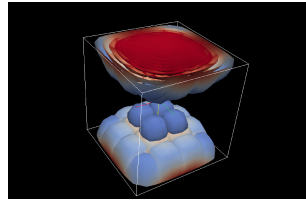
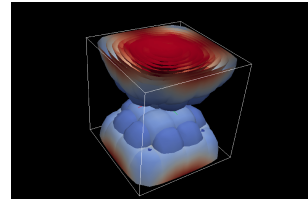
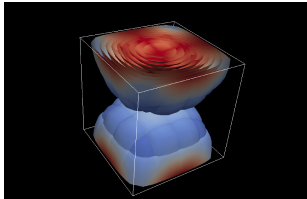
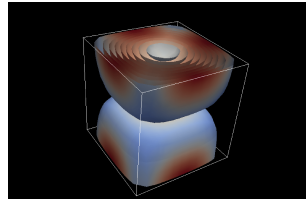
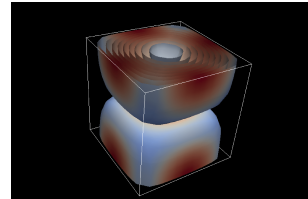
Fig. 5.7: Convergence history for the iHDG method with upwind and NPC fluxes for $\kappa = 10^{-3}$ (top row) and $\kappa = 10^{-6}$ (bottom row).

In table 5.4 we compare the number of iterations the iHDG algorithm takes to converge for $\nu = \{1, 10\}$ cases. Note that “*” indicates that the scheme either reaches 2000 iterations or diverges. The convergent condition $h > Q_1$ in section 4.2 is equivalent to $h > \mathcal{O}\left(\frac{1}{\sqrt{\lambda}}\right)$ and since $\sqrt{\lambda} = \sqrt{\nu}$ we see similar convergence/divergence behavior for both $\nu = 1$ and 10 (because the lower bound for h is of the same order for these cases). For $\nu = 100$ the lower bound for h is one order of magnitude smaller, and this allows us to obtain convergence for two additional cases: i) $N_{el} = 512$ and $p = 4$ with 1160 iterations; and ii) $N_{el} = 4096$ and $p = 2$ with 1450 iterations.

Figure 5.8 shows the convergence history for different meshes and solution orders for $\nu = 1$ and $\nu = 10$. We notice that the convergence trend is different from the pure convection and convection-diffusion cases, that is, it is exponential in the number of iterations starting from the beginning, but the rate is less. We also show in Figure 5.9 the evolution of σ with respect to the number of iterations for $N_{el} = 64$ and solution order $p = 4$. Unlike the convection (or convection-dominated) case, the convergence of the iHDG solution for the elliptic PDE does not have a preferable direction.

Table 5.4: The number of iHDG iterations for $\nu = 1$ and $\nu = 10$ with $\tau = \frac{(p+1)(p+2)}{h}$.

N_{el}	$\nu = 1$				$\nu = 10$			
	$p = 1$	$p = 2$	$p = 3$	$p = 4$	$p = 1$	$p = 2$	$p = 3$	$p = 4$
8	4	24	60	98	3	17	54	90
64	37	119	285	569	32	108	249	497
512	158	527	1296	*	130	429	1124	*
4096	1519	*	*	*	1178	*	*	*

(a) $\nu = 1$ (b) $\nu = 10$ Fig. 5.8: Convergence of the iHDG algorithm for different mesh size h and solution order $p = \{3, 4\}$ for 3D elliptic equation with $\nu = 1$ and $\nu = 10$.(a) σ at iteration = 1(b) σ at iteration = 10(c) σ at iteration = 20(d) σ at iteration = 30(e) σ at iteration = 90(f) σ at iteration = 569Fig. 5.9: Evolution of σ with respect to the number of iterations for $\nu = 1$.

5.4. Time dependent convection-diffusion equation. In this section we consider the following equation

$$\kappa^{-1}\boldsymbol{\sigma}^e + \nabla u^e = 0 \quad \text{in } \Omega, \quad (5.5a)$$

$$\frac{\partial u^e}{\partial t} + \nabla \cdot \boldsymbol{\sigma}^e + \boldsymbol{\beta} \cdot \nabla u^e = 0 \quad \text{in } \Omega. \quad (5.5b)$$

We are interested in the transport of the contaminant concentration [1, 34] with diffusivity $\kappa = 0.01$ in a three dimensional domain $\Omega = [0, 5] \times [-1.25, 1.25] \times [-1.25, 1.25]$ with convective velocity field $\boldsymbol{\beta}$ given as⁸

$$\boldsymbol{\beta} = \left(1 - e^{\gamma x} \cos(2\pi y), \frac{\gamma}{2\pi} e^{\gamma x} \sin(2\pi y), 0 \right),$$

where $\gamma = \frac{Re}{2} - \sqrt{\frac{Re^2}{4} + 4\pi^2}$ and $Re = 100$. Starting from $t = 0$, and for every second afterwards, the same distribution of contaminant concentration of the form

$$u_0 = e^{\frac{(x-1)^2 + y^2 + z^2}{0.5^2}} + e^{\frac{(x-1)^2 + (y-0.5)^2 + z^2}{0.5^2}} + e^{\frac{(x-1)^2 + (y+0.5)^2 + z^2}{0.5^2}}$$

is injected into the flow field. A time stepsize of $\Delta t = 0.025$ is selected and the simulation is run for 400 time steps, i.e. till $T = 10$, with the Crank-Nicolson method. Here, we use the mesh with $N_{el} = 512$ elements and solution order $p = 4$. On the left boundary, i.e. $x = 0, -1.25 \leq y \leq 1.25, -1.25 \leq z \leq 1.25$, the Dirichlet boundary condition $u = 0$ is applied, while on the remaining boundary faces, we employ the homogeneous Neumann boundary condition $\nabla u \cdot \mathbf{n} = 0$. The Peclet number for this problem is 200. This exhibits a wide range of mixed hyperbolic and parabolic regimes and hence is a good test bed for the proposed iHDG scheme. In this example, the iHDG algorithm with NPC flux does not converge even for coarse meshes and low solution orders (this can be seen in section 5.3). We therefore show numerical results only for the upwind HDG flux in Figure 5.10. The scheme requires approximately 46 iterations for each time step to reach the stopping criteria $\|u^k - u^{k-1}\|_{L^2} < 10^{-6}$. Since $\nabla \cdot \boldsymbol{\beta} = 0$ and $\lambda = 1/\Delta t$ (see remark 4.2) we obtain from section 4.2 the estimate for the upwind flux: $\Delta t = \mathcal{O}\left(\frac{h}{(p+1)(p+2)}\right)$. Using this estimate we compare the number of iterations the iHDG algorithm takes to converge for different meshes and solution orders. We do not obtain convergence for $N_{el} = 4096$ and solution orders equal to 3 and 4: the main reason is that this problem is in the mixed hyperbolic and parabolic regime and the above setting does not satisfy the condition for convergence (see Section 5.3).

6. Conclusions and Future Work. We have presented an iterative solver, namely iHDG, for HDG discretizations of linear PDEs. The method exploits the structure of HDG discretization and idea from domain decomposition methods. One of the key features of the iHDG solver is that it only requires local solves, element-by-element completely independent of each other, during each iteration. Using an energy approach we rigorously derive the conditions under which the iHDG algorithm is convergent for transport equation, linearized shallow water equation, and convection-diffusion equation. In particular, for scalar transport equation, the algorithm is convergent for all meshes and solution orders, and the convergence rate is independent of solution order. This feature makes the iHDG solver especially suitable for high-order

⁸Here, $\boldsymbol{\beta}$ is an extension of 2D analytical solution of Kovasznay flow [27].

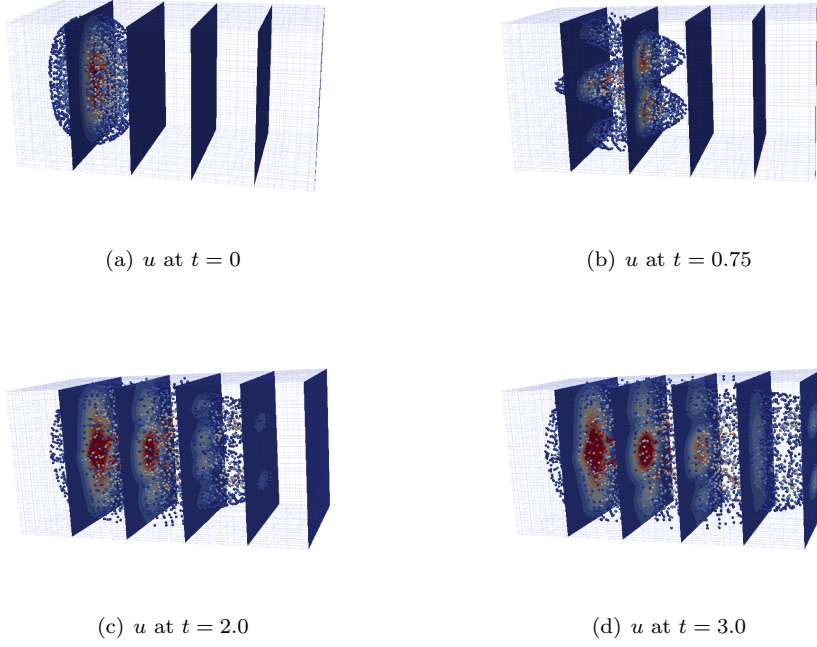


Fig. 5.10: Solution u as a function of time using the iHDG algorithm with the upwind flux for the contaminant transport problem (5.5).

Table 5.5: The number of iHDG iterations per time step for the contaminant transport problem with various solution orders and mesh sizes.

N_{el}	$p = 1$	$p = 2$	$p = 3$	$p = 4$
8	12	24	23	22
64	26	26	22	20
512	21	23	17	37
4096	17	18	*	*

DG methods, that is, high-order (and hence more accurate) solutions do not require more number of iterations. The scheme in fact performs an implicit matching and the solution converges in patches of elements from the inflow to the outflow boundaries. For the linearized shallow water equation, we prove that the convergence is conditional on the mesh size and the solution order. Similar conditional convergence is also shown for the convection-diffusion equation in the first order form. We have studied the performance of the scheme in convection dominated, mixed (hyperbolic-elliptic) and diffusion regimes and numerically verified our theoretical results. Ongoing work is to improve the convergence of the iHDG scheme for diffusion-dominated problems. We are also exploring the opportunity to employ the iHDG solver as a preconditioner for Krylov subspace methods or as scalable smoother for multigrid solvers.

Acknowledgements. The authors would like to thank Dr. Jeonghun J. Lee for fruitful discussions. We are indebted to Dr. Hari Sundar for sharing his high-order finite element library **homg**, on which we have implemented the iHDG algorithms and produced numerical results.

REFERENCES

- [1] O. BASHIR, K. WILLCOX, O. GHATTAS, B. VAN BLOEMEN WAANDERS, AND J. HILL, Hessian-based model reduction for large-scale systems with initial condition inputs, International Journal for Numerical Methods in Engineering, 73 (2008), pp. 844–868.
- [2] D. BENNEQUIN, M. J. GANDER, AND L. HALPERN, A homographic best approximation problem with application to optimized Schwarz waveform relaxation, Math. Comp., 78 (2009), pp. 185–223.
- [3] T. BUI-THANH, From Godunov to a unified hybridized discontinuous Galerkin framework for partial differential equations, Journal of Computational Physics, 295 (2015), pp. 114–146.
- [4] ———, From Rankine-Hugoniot Condition to a Constructive Derivation of HDG Methods, Lecture Notes in Computational Sciences and Engineering, Springer, 2015, pp. 483–491.
- [5] TAN BUI-THANH, Hybridized discontinuous Galerkin methods for linearized shallow water equations, Submitted, (2015).
- [6] JESSE CHAN, NORBERT HEUER, TAN BUI-THANH, AND LESZEK DEMKOWICZ, A robust dpg method for convection-dominated diffusion problems ii: Adjoint boundary conditions and mesh-dependent test norms, Computers & Mathematics with Applications, 67 (2014), pp. 771–795.
- [7] B. COCKBURN, B. DONG, J. GUZMAN, M. RESTELLI, AND R. SACCO, A hybridizable discontinuous Galerkin method for steady state convection-diffusion-reaction problems, SIAM J. Sci. Comput., 31 (2009), pp. 3827–3846.
- [8] B. COCKBURN AND J. GOPALAKRISHNAN, The derivation of hybridizable discontinuous Galerkin methods for Stokes flow, SIAM J. Numer. Anal., 47 (2009), pp. 1092–1125.
- [9] BERNARDO COCKBURN, JAY GOPALAKRISHNAN, AND RAYTCHO LAZAROV, Unified hybridization of discontinuous Galerkin, mixed, and continuous Galerkin methods for second order elliptic problems, SIAM J. Numer. Anal., 47 (2009), pp. 1319–1365.
- [10] BERNARDO COCKBURN, JAY GOPALAKRISHNAN, AND FRANCISCO-JAVIER SAYAS, A projection-based error analysis of HDG methods, Mathematics Of Computation, 79 (2010), pp. 1351–1367.
- [11] BERNARDO COCKBURN, GEORGE E. KARNIADAKIS, AND CHI-WANG SHU, Discontinuous Galerkin Methods: Theory, Computation and Applications, Lecture Notes in Computational Science and Engineering, Vol. 11, Springer Verlag, Berlin, Heidelberg, New York, 2000.
- [12] J. CUI AND W. ZHANG, An analysis of HDG methods for the Helmholtz equation, IMA J. Numer. Anal., 34 (2014), pp. 279–295.
- [13] H. EGGER AND J. SCHOBERL, A hybrid mixed discontinuous Galerkin finite element method for convection-diffusion problems, IMA Journal of Numerical Analysis, 30 (2010), pp. 1206–1234.
- [14] M. J. GANDER, On the influence of geometry on optimized Schwarz methods, SeMA J., (2011), pp. 71–78.
- [15] MARTIN J. GANDER, LOÏC GOUARIN, AND LAURENCE HALPERN, Optimized Schwarz waveform relaxation methods: a large scale numerical study, in Domain decomposition methods in science and engineering XIX, vol. 78 of Lect. Notes Comput. Sci. Eng., Springer, Heidelberg, 2011, pp. 261–268.
- [16] MARTIN J. GANDER AND SOHEIL HAJIAN, Analysis of Schwarz methods for a hybridizable discontinuous Galerkin discretization, SIAM J. Numer. Anal., 53 (2015), pp. 573–597.
- [17] MARTIN J. GANDER, LAURENCE HALPERN, AND KÉVIN SANTUGINI REPIQUET, Non shape regular domain decompositions: an analysis using a stable decomposition in H_0^1 , in Domain decomposition methods in science and engineering XX, vol. 91 of Lect. Notes Comput. Sci. Eng., Springer, Heidelberg, 2013, pp. 485–492.
- [18] MARTIN J. GANDER AND FELIX KWOK, Best Robin parameters for optimized Schwarz methods at cross points, SIAM J. Sci. Comput., 34 (2012), pp. A1849–A1879.
- [19] F. X. GIRALDO AND T. WARBURTON, A high-order triangular discontinuous Galerkin oceanic shallow water model, International Journal For Numerical Methods In Fluids, 56 (2008), pp. 899–925.
- [20] A. GREENBAUM, Iterative Methods for the Solution of Linear Systems, SIAM, Philadelphia,

- 1997.
- [21] R. GRIESMAIER AND P. MONK, Error analysis for a hybridizable discontinuous Galerkin method for the Helmholtz equation, J. Sci. Comput., 49 (2011), pp. 291–310.
 - [22] LAURENCE HALPERN, Optimized Schwarz waveform relaxation: roots, blossoms and fruits, in Domain decomposition methods in science and engineering XVIII, vol. 70 of Lect. Notes Comput. Sci. Eng., Springer, Berlin, 2009, pp. 225–232.
 - [23] LAURENCE HALPERN AND JÉRÉMIE SZEFTTEL, Nonlinear nonoverlapping Schwarz waveform relaxation for semilinear wave propagation, Math. Comp., 78 (2009), pp. 865–889.
 - [24] PAUL HOUSTON, DOMINIK SCHÖTZAU, AND XIAOXI WEI, A mixed DG method for linearized incompressible magnetohydrodynamics, J. Sci. Comput., 40 (2009), pp. 281–314.
 - [25] C. JOHNSON AND J. PITKÄRANTA, An analysis of the discontinuous Galerkin method for a scalar hyperbolic equation, Mathematics of Computation, 46 (1986), pp. 1–26.
 - [26] R. M. KIRBY, S. J. SHERWIN, AND B. COCKBURN, To CG or to HDG: A comparative study, J. Sci. Comput., 51 (2012), pp. 183–212.
 - [27] L. I. G. KOVASZNAY, Laminar flow behind a two-dimensional grid, Mathematical Proceedings of the Cambridge Philosophical Society, 44 (1948), pp. 58–62.
 - [28] P. LESANT AND P. A. RAVIART, On a finite element method for solving the neutron transport equation, in Mathematical Aspects of Finite Element Methods in Partial Differential Equations, C. de Boor, ed., Academic Press, 1974, pp. 89–145.
 - [29] L. LI, S. LANTERI, AND R. PERRUSSEL, A hybridizable discontinuous Galerkin method for solving 3D time harmonic Maxwell’s equations, in Numerical Mathematics and Advanced Applications 2011, Springer, 2013, pp. 119–128.
 - [30] P.-L. LIONS, On the Schwarz alternating method. I, in First International Symposium on Domain Decomposition Methods for Partial Differential Equations (Paris, 1987), SIAM, Philadelphia, PA, 1988, pp. 1–42.
 - [31] ———, On the Schwarz alternating method. II. Stochastic interpretation and order properties, in Domain decomposition methods (Los Angeles, CA, 1988), SIAM, Philadelphia, PA, 1989, pp. 47–70.
 - [32] ———, On the Schwarz alternating method. III. A variant for nonoverlapping subdomains, in Third International Symposium on Domain Decomposition Methods for Partial Differential Equations (Houston, TX, 1989), SIAM, Philadelphia, PA, 1990, pp. 202–223.
 - [33] D. MORO, N. C. NGUYEN, AND J. PERAIRE, Navier-Stokes solution using hybridizable discontinuous Galerkin methods, American Institute of Aeronautics and Astronautics, 2011-3407 (2011).
 - [34] N. C. NGUYEN, J. PERAIRE, AND B. COCKBURN, An implicit high-order hybridizable discontinuous Galerkin method for linear convection-diffusion equations, Journal Computational Physics, 228 (2009), pp. 3232–3254.
 - [35] ———, A hybridizable discontinuous Galerkin method for Stokes flow, Comput Method Appl. Mech. Eng., 199 (2010), pp. 582–597.
 - [36] ———, High-order implicit hybridizable discontinuous Galerkin method for acoustics and elastodynamics, Journal Computational Physics, 230 (2011), pp. 3695–3718.
 - [37] ———, Hybridizable discontinuous Galerkin method for the time harmonic Maxwell’s equations, Journal Computational Physics, 230 (2011), pp. 7151–7175.
 - [38] ———, An implicit high-order hybridizable discontinuous Galerkin method for the incompressible Navier-Stokes equations, Journal Computational Physics, 230 (2011), pp. 1147–1170.
 - [39] W. H. REED AND T. R. HILL, Triangular mesh methods for the neutron transport equation, Tech. Report LA-UR-73-479, Los Alamos Scientific Laboratory, 1973.
 - [40] YOUSEF SAAD, Iterative methods for sparse linear systems, Society for Industrial and Applied Mathematics, Philadelphia, PA, second ed., 2003.
 - [41] MINH-BINH TRAN, Parallel Schwarz waveform relaxation method for a semilinear heat equation in a cylindrical domain, C. R. Math. Acad. Sci. Paris, 348 (2010), pp. 795–799.
 - [42] ———, Parallel Schwarz waveform relaxation algorithm for an N -dimensional semilinear heat equation, ESAIM Math. Model. Numer. Anal., 48 (2014), pp. 795–813.
 - [43] T. WARBURTON AND J. S. HESTHAVEN, On the constants in hp -finite element trace inverse inequalities, Comput. Methods Appl. Mech. Engrg., 192 (2003), pp. 2765–2773.